nature methods

Article

https://doi.org/10.1038/s41592-023-01880-5

Engineered allostery in light-regulated LOV-Turbo enables precise spatiotemporal control of proximity labeling in living cells

Received: 14 November 2022

Accepted: 14 April 2023

Published online: 15 May 2023

Check for updates

Song-Yi Lee[1,8], Joleen S. Cheah[2,8], Boxuan Zhao[1], Charles Xu[3], Heegwang Roh[4], Christina K. Kim[1,6], Kelvin F. Cho[1,7], Namrata D. Udeshi[3], Steven A. Carr[3] & Alice Y. Ting[1,2,4,5]

The incorporation of light-responsive domains into engineered proteins has enabled control of protein localization, interactions and function with light. We integrated optogenetic control into proximity labeling, a cornerstone technique for high-resolution proteomic mapping of organelles and interactomes in living cells. Through structure-guided screening and directed evolution, we installed the light-sensitive LOV domain into the proximity labeling enzyme TurboID to rapidly and reversibly control its labeling activity with low-power blue light. 'LOV-Turbo' works in multiple contexts and dramatically reduces background in biotin-rich environments such as neurons. We used LOV-Turbo for pulse-chase labeling to discover proteins that traffic between endoplasmic reticulum, nuclear and mitochondrial compartments under cellular stress. We also showed that instead of external light, LOV-Turbo can be activated by bioluminescence resonance energy transfer from luciferase, enabling interaction-dependent proximity labeling. Overall, LOV-Turbo increases the spatial and temporal precision of proximity labeling, expanding the scope of experimental questions that can be addressed with proximity labeling.

Many natural enzymes are controlled by allosteric regulation. Binding by a ligand, RNA or protein at a distal site leads to conformational changes that are transmitted, sometimes over long distances, to the enzyme's active site to alter its catalytic properties[1]. Among engineered enzymes, however, allostery is far less common[2–4]. Although allosteric control could improve the spatial and/or temporal precision of many engineered enzymes and enable input-dependent activity that could be exploited for synthetic circuit design, there are few systematic approaches for introducing engineered allostery into enzymes of interest.

Here we report the engineering of a light-regulated variant of TurboID via the introduction of designed allostery. TurboID is an artificial enzyme used for promiscuous proximity-dependent biotinylation in living cells and mapping of spatial proteomes[5]. Engineered via directed evolution from the *Escherichia coli* enzyme biotin ligase (BirA), TurboID uses biotin and ATP to generate a reactive biotinyl-AMP mixed anhydride that it releases from its active site to covalently tag nearby proteins on nucleophilic lysine sidechains. While TurboID has been used extensively for mapping interactomes and organelle proteomes in culture and in vivo[6,7], it does have important limitations. First, TurboID activity is most commonly controlled by the availability of its substrate, biotin, which is endogenously present in most living organisms, contributing to background labeling before exogenous biotin addition

[1]Department of Genetics, Stanford University, Stanford, CA, USA. [2]Department of Biology, Stanford University, Stanford, CA, USA. [3]Broad Institute of MIT and Harvard, Cambridge, MA, USA. [4]Department of Chemistry, Stanford University, Stanford, CA, USA. [5]Chan Zuckerberg Biohub–San Francisco, San Francisco, CA, USA. [6]Present address: Center for Neuroscience and Department of Neurology, University of California, Davis, CA, USA. [7]Present address: Amgen Research, South San Francisco, CA, USA. [8]These authors contributed equally: Song-Yi Lee, Joleen S. Cheah. e-mail: ayting@stanford.edu

and consequently, limited temporal specificity. Second, the spatial specificity of TurboID (and all other proximity labeling enzymes) is determined by the quality of its genetic targeting, which is sometimes insufficiently specific for the cell type, cellular subcompartment or protein complex of interest.

To address these limitations, we report a light-regulated variant of TurboID, 'LOV-Turbo', a single 50 kDa polypeptide that has nearly undetectable activity in the dark state but turns on within seconds of weak blue light illumination to give activity comparable to that of TurboID. We show that LOV-Turbo improves the spatial and temporal precision of proximity labeling in culture and in vivo, and enables new applications not possible with TurboID, including pulse-chase labeling to map proteome dynamics in living systems. Furthermore, our study demonstrates a semirational approach to engineering light-induced allostery with an extremely high dynamic range that could be applied to other enzymes of interest.

Results

Design of light-regulated TurboID or LOV-Turbo

Light is a versatile input that can be delivered in a spatially and temporally precise manner, even in vivo. A light-regulated version of TurboID would enable precise control over the time window of proteome labeling as well as its location. We sought to introduce light regulation to TurboID with several design goals in mind. First, we envisioned a single protein construct, rather than a multicomponent system, for ease of use and robust performance across a range of expression levels. Second, to be maximally effective, light-regulated TurboID should have negligible 'leak' or background activity in the dark state and activity comparable to that of the parent TurboID enzyme in the presence of light. Third, light-regulated TurboID should be rapidly reversible, so that activity can be shut off after the desired labeling period, enabling 'chase' experiments to be performed. Last, the illumination conditions required for TurboID activation should be mild (around 1 mW cm^{-2}), so that specialized equipment is not needed and phototoxicity is minimal.

To meet these criteria, we envisioned integrating the LOV photosensory domain, a 16 kDa flavin-containing protein from the *Avena sativa* oat plant, into TurboID to regulate its activity with light. The core of LOV forms a tight complex, or 'clamp', with its C-terminal Jα helix in the dark state but releases the Jα helix in the presence of blue 470 nm light (Fig. 1a). The light power required is extremely low; cell cultures containing the LOV domain can often be stimulated by ambient room light.

By inserting LOV into a surface-exposed loop of TurboID that is allosterically coupled to its active site, we envisioned distorting and impairing the active site through LOV's clamping effect in the dark state but releasing it to a 'native-like' and active conformation on illumination. To test this possibility, we selected nine different surface-exposed loops in TurboID, based on the crystal structure of the parent enzyme BirA[8], and explored 1–6 different LOV insertion sites in each loop (Supplementary Fig. 1a). A total of 31 insertion sites were tested, using the hybrid LOV domain (hLOV1 (ref. 9)) that exhibits a combination of high signal in the light state and minimal leak in the dark state when used in other optogenetic tools such as FLiCRE[10] and SPARK[9].

Out of 31 sites we tested, 12 eliminated TurboID activity altogether and another five impaired activity in both light and dark states (Fig. 1b and Supplementary Fig. 1a). One site (141/142) showed light-dependent activity, but in the opposite direction to what we desired (activity inhibited by light). A single fusion construct showed increased activity after light exposure: the 80/81 LOV insertion, between the fourth α-helix and a mixed β-sheet of TurboID. In general, we found that loops closer to TurboID's N terminus were better able to tolerate LOV insertion than loops near the C terminus. Also, insertion sites designed to block the biotin-binding pocket resulted in a complete loss of TurboID activity.

We further optimized the 80/81 LOV-Turbo fusion to improve the ±light signal ratio. The addition of Gly-Ser linkers N-terminal to the LOV domain had no effect, while Gly-Ser linkers inserted C-terminal to LOV, after the Jα helix, were deleterious for light-dependence (Supplementary Fig. 1b). Even a single glycine inserted after Jα abolished the light-dependent activity of LOV-Turbo. Given this sensitivity, we hypothesized that it might be beneficial to further shorten the LOV insertion region. We did so by truncating the 80/81 loop into which the LOV domain was inserted, removing 1–6 amino acids N-terminal to Gly80. Removal of four amino acids decreased dark state activity while maintaining light-state activity (Fig. 1c), giving a more than twofold improvement in ±light signal ratio.

This optimized construct, named LOV-Turbo1, was effective in cells, but we found that its expression level was considerably lower than that of TurboID, indicating instability and limiting the levels of achievable biotinylation (Supplementary Fig. 1c). To address this problem, we turned to directed evolution, both to improve LOV-Turbo1's expression and stability, and to further optimize its dynamic range.

Directed evolution of LOV-Turbo

We selected yeast display as our directed evolution platform for LOV-Turbo, as it has previously been used to evolve TurboID[5] and APEX2 (ref. 11). We further modified the platform to incorporate alternating rounds of positive selection in light and negative selection in the dark (Fig. 1d). By this approach, we hoped to enrich LOV-Turbo variants with a high dynamic range as well as robust cell surface expression.

We used error-prone PCR to introduce mutations throughout the LOV-Turbo1 template. Sequencing showed an average mutation rate of 1.4 amino acids per gene in our library. Roughly 10^7 LOV-Turbo variants were displayed on the yeast surface as a fusion to the Aga2p mating protein. We performed labeling with biotin and ATP in the presence of light for 90 min, before washing and staining with streptavidin-phycoerythrin (SA-PE) to detect self-biotinylation, and anti-Myc antibody staining to quantify LOV-Turbo expression level. Approximately 38% of our initial library had detectable biotinylation activity under these conditions, with a mean activity around twofold lower than that of LOV-Turbo1, indicating a good level of mutagenesis and library diversity.

We performed three rounds of positive selection, followed by two rounds of negative selection in the dark, enriching clones that had low streptavidin but high-Myc staining under these conditions. Last, we performed two more rounds of positive selection, but at 37 °C rather than the typical 30 °C yeast culturing conditions to increase selection stringency for stable and well-folded clones (Fig. 1e and Supplementary Fig. 1d). Fluorescence-activated cell sorting (FACS) plots in Fig. 1f show that our final round seven yeast pool displays both higher expression and higher promiscuous biotinylation activity than the template, LOV-Turbo1. Sequencing of clones from this pool showed mutations in both the LOV domain and the TurboID gene, with T52S, I147T, I231V and F286L mutations especially enriched (Supplementary Table 1). As shown in Fig. 2a, these mutations are distributed across the LOV-Turbo predicted structure, with some proximal to the biotin-binding site, and others in the N-terminal domain, far from the active site.

We characterized 19 clones from round seven on the yeast surface (Supplementary Fig. 1e) and selected eight for analysis in human embryonic kidney (HEK) 293T cells. All showed light-dependent activity in the HEK cytosol, but to varying degrees (Fig. 1g and Supplementary Fig. 1f). We used this data to guide the selection of mutations for manual recombination, generating another 13 LOV-Turbo variants (C1–C13, Fig. 1h and Supplementary Fig. 1g,h). Testing of these alongside yeast-enriched clones revealed that C10, with six mutations in the TurboID sequence and no mutations in the LOV domain, showed higher ±light signal ratio and expression level than LOV-Turbo1 template under matched conditions. The AlphaFold[12]-predicted structure of C10 (Fig. 2a) shows that its six mutations are distributed across the entire protein, with only two (I231V and A166V) close to the biotin/ATP substrate binding pockets. Other mutations may contribute to C10's improved expression.

https://doi.org/10.1038/s41592-023-01880-5

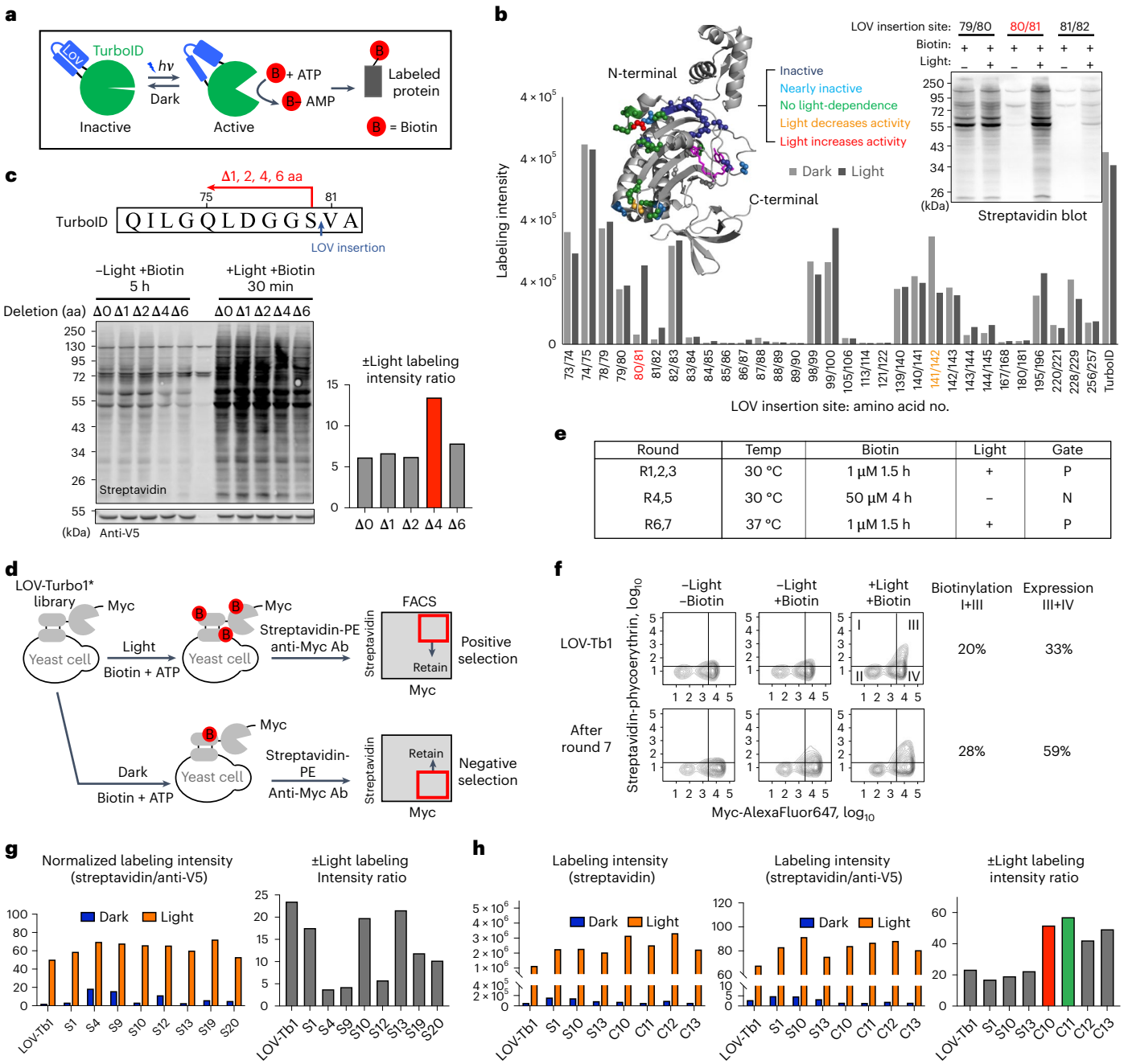

Fig. 1 | Design and directed evolution of LOV-Turbo. a, LOV-Turbo has a blue-light-sensitive hLOV1 (ref. 9) domain inserted into its sixth surface-exposed loop (domain structure shown in Supplementary Fig. 1a). In the dark state, clamping by hLOV1 keeps TurboID inactive, while in the light state, clamp release restores TurboID activity. Active LOV-Turbo promiscuously biotinylates nearby proteins, enabling their identification by mass spectrometry. **b**, Screening of 31 LOV insertion sites in TurboID. Constructs were expressed in the HEK cytosol and labeling was performed for 30 min in light or dark. Relative biotinylation activity was quantified by streptavidin blotting of whole-cell lysates. Multiple blots were quantified parallel by normalizing with TurboID biotinylation intensity. Inset shows sample data. Ribbon structure of BirA (PDB ID 2EWN) shows LOV insertion sites and the result obtained for each. Nonhydrolyzable biotinol-5′-AMP in pink. This experiment was performed once, except the 80/81 and 141/142 constructs, which were performed twice with similar results. **c**, Truncation of LOV-TurboID at the 80/81 insertion site improves light gating. Amino acids (aa) 75–80 were progressively truncated as shown. The Δ4 construct showed the highest ± light signal ratio and lowest-light leak. This experiment was performed twice with similar results. **d**, Scheme for directed evolution on the yeast cell surface. PE, phycoerythrin. Ab, antibody. **e**, Selection conditions used over seven rounds. Positive selection (P) and negative selection (N) gates are shown in **d**. **f**, FACS plots comparing LOV-Turbo1 template to postround seven yeast population. Percentages give fractions of active cells (in quadrants I + III) and fractions of expressing cells (in quadrants III + IV). **g**, Screening of eight evolved mutants in the HEK cytosol. Biotinylation intensity quantified by streptavidin blot of whole-cell lysates (shown in Supplementary Fig. 1f), after labeling for 30 min in light or 5 h in dark. LOV-Tb1, LOV-Turbo1. **h**, Same as **g** but with combination mutants C10-C13 as well, after labeling for 30 min in light or 4 h in dark. Blots are shown in Supplementary Fig. 1h. C10 was selected over C11 as our final LOV-Turbo due to its higher expression level in HEK 293T cells.

https://doi.org/10.1038/s41592-023-01880-5

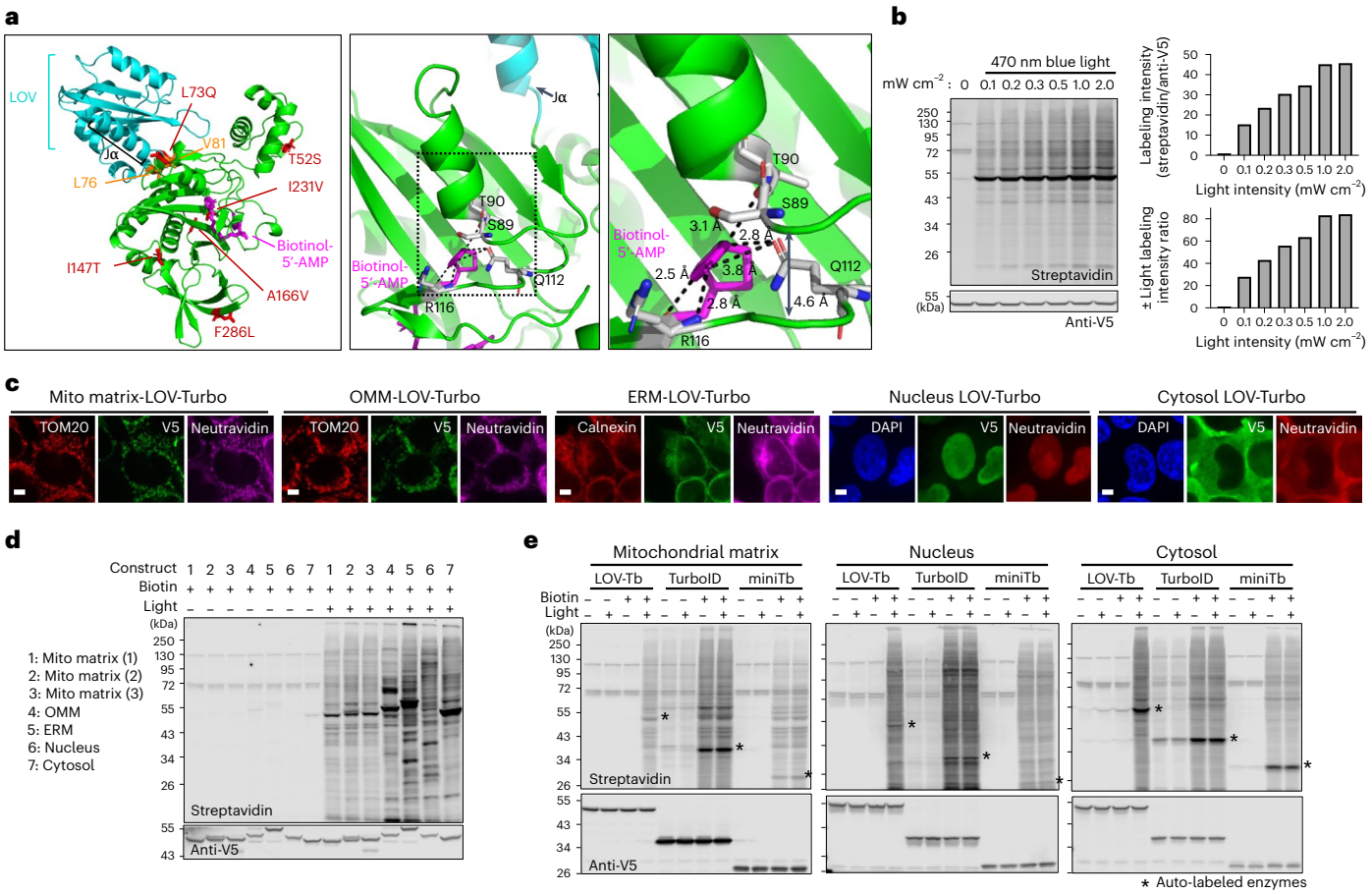

Fig. 2 | Characterization of LOV-Turbo. a, AlphaFold-predicted structure of evolved LOV-Turbo (clone C10). LOV domain in cyan and TurboID in green. L76 and V81 flanking the LOV insertion site are colored orange. The six mutations enriched by directed evolution are colored red. Nonhydrolyzable biotinol-5′-AMP in pink. Close-up views show TurboID's active site in relation to residues that may be allosterically coupled to the LOV domain. Double-headed arrow shows the distance between indicated backbone loops. **b**, Light intensity-dependence of LOV-Turbo. HEK 293T cells expressing LOV-Turbo in the cytosol were stimulated with blue light of varying intensities (0.1–1 mW cm^{-2}) for 15 min in the presence of biotin. Lysates were analyzed by streptavidin and anti-V5 blotting. This experiment was performed once. **c**, Confocal imaging of LOV-Turbo-catalyzed biotinylation in the mitochondrial matrix, outer mitochondrial membrane (OMM), ERM facing the cytosol, nucleus and cytosol. Anti-V5 detects LOV-Turbo expression. Neutravidin-AF647 detects biotinylated proteins, after 30 min of labeling under blue light illumination. TOM20 and calnexin are endogenous mitochondrial and ER markers, respectively. DAPI stains the nucleus. Scale bars, 5 µm. This experiment was performed twice with similar results. **d**, Streptavidin blotting of HEK 293T lysates expressing LOV-Turbo targeted to various compartments and labeled with biotin and blue light for 30 min. Three different mitochondrial matrix targeting sequences were tested (Methods). This experiment was performed once. **e**, Comparison of LOV-Turbo (LOV-Tb), TurboID and miniTurbo (miniTb) in HEK mitochondrial matrix, nucleus and cytosol. Labeling time was 30 min. The * indicates auto-labeled LOV-Turbo, TurboID or miniTurbo. This experiment was performed once.

Using C10 as a template, we also tested whether swapping out the entire hLOV1 domain for other published LOV domains could improve performance. Supplementary Fig. 1i shows that only iLID[13,14] and variants of hLOV (f-hLOV1, ref. 10 (I25V or V14T)[15] and hLOV1, ref. 9), which are known to exhibit tight caging in the dark state, gave strong light gating. Wild-type AsLOV2 and eLOV[16] constructs exhibited dark state leak. Ultimately, our original C10 with hLOV1 remained superior. We selected C10 as our final optimized LOV-Turbo, henceforth it is named 'LOV-Turbo'.

Characterization of LOV-Turbo in mammalian cells

To characterize LOV-Turbo, we performed a labeling time course in the HEK cytosol as well as a titration of biotin concentration. With 100 µM exogenous biotin, we observed a steady increase in promiscuous labeling over 120 min, with not much increase in signal beyond 150 min (Supplementary Fig. 2a). The labeling after 10 min was comparable to that of TurboID and exceeded the signal from miniTurbo[5], suggesting that the standard labeling time of 10 min used for TurboID should be suitable for LOV-Turbo as well (Supplementary Fig. 2b). We could barely detect promiscuous labeling in the dark state, even at the highest biotin concentration of 0.5 mM or when cells were incubated with 100 µM biotin overnight (Supplementary Fig. 2c,d). As expected, LOV-Turbo can be activated by 470 nm blue light, but not 660 nm red light, which facilitates the handling of LOV-Turbo samples in red light-illuminated dark rooms (Supplementary Fig. 2e). We performed a study of LOV-Turbo light requirements and found the best turn-on with continuous illumination at 1 mW cm^{-2} power (Fig. 2b). Alternatively, 10–1,000 ms pulses of 2.5 mW cm^{-2} light at a 33% duty cycle give a comparable degree of activation (Supplementary Fig. 2f,g).

We next probed LOV-Turbo performance across multiple subcellular compartments in HEK 293T cells (Fig. 2c–e). We observed strong light- and biotin-dependent labeling in the cytosol, nucleus, mitochondrial matrix, outer mitochondrial membrane and endoplasmic reticulum (ER) membrane facing the cytosol. Each compartment gave a unique 'fingerprint' by streptavidin blotting, reflective of the different subcellular proteomes tagged by LOV-Turbo in each location

https://doi.org/10.1038/s41592-023-01880-5

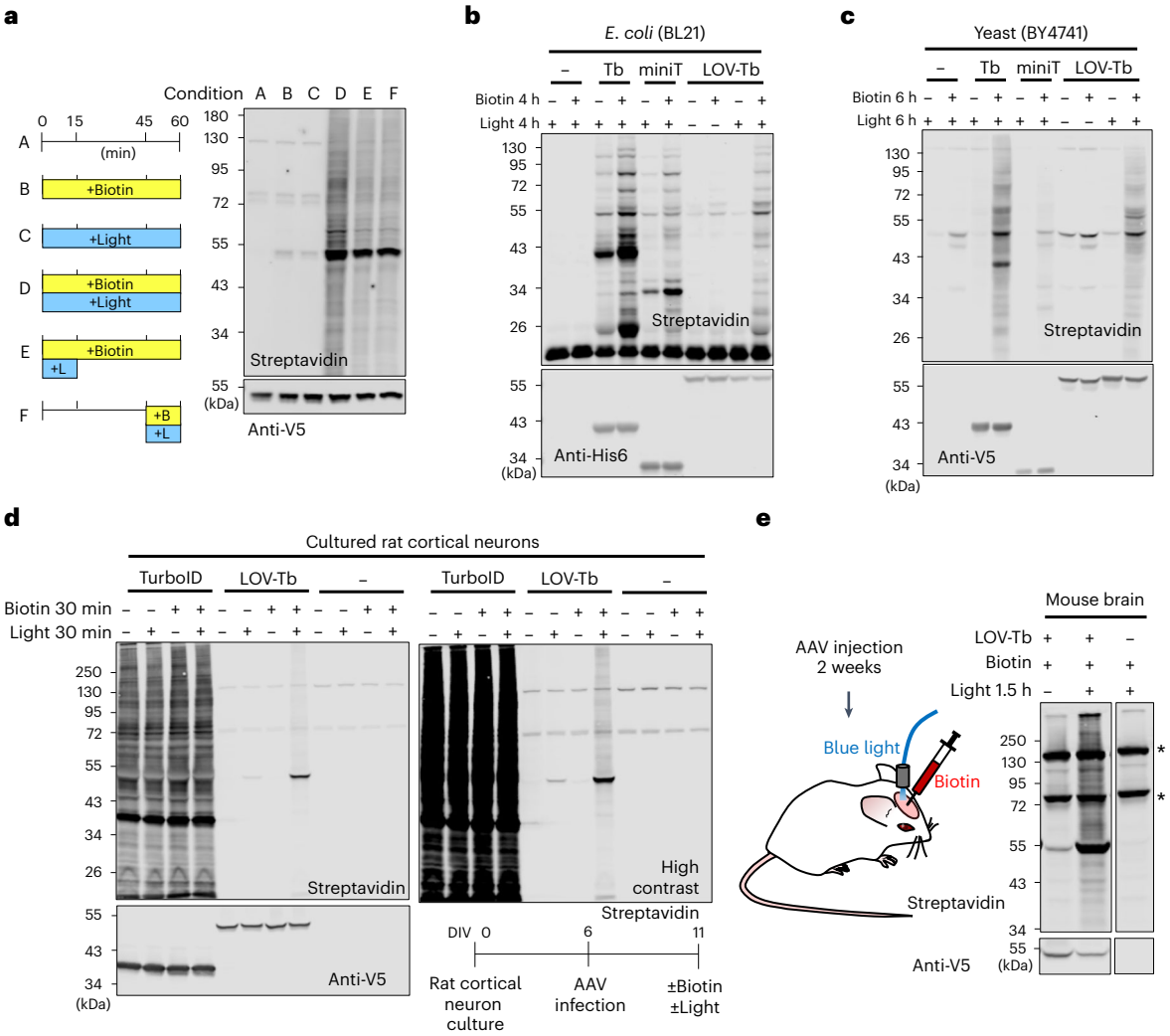

Fig. 3 | LOV-Turbo is reversible and works in multiple cell types and in the rodent brain. a, LOV-Turbo labeling is terminated by the removal of light. HEK 293T cells expressing LOV-Turbo in the cytosol were labeled as shown in conditions A–F. Whole-cell lysates were then analyzed by streptavidin blotting. This experiment was performed twice with similar results. **b**, LOV-Turbo labeling in *E. coli*. Constructs were expressed in the cytosol of BL21 *E. coli* and labeling was performed for 4 h. Anti-His_6 antibody detects ligase expression. Tb, TurboID. miniT, miniTurbo. This experiment was performed once. **c**, LOV-Turbo labeling in yeast (BY4741 strain). Labeling was performed for 6 h. This experiment was performed once. **d**, LOV-Turbo labeling in cultured rat cortical neurons. LOV-Turbo or TurboID was expressed in the cytosol via adeno-associated virus 1/2 (AAV) infection for 5 days before labeling. TurboID shows high background even without exogenous biotin addition. This experiment was performed once. **e**, LOV-Turbo labeling in the mouse brain. Cytosolic LOV-Turbo was expressed in the mouse cortex via AAV1/2 injection. 2 weeks later, 0.5 µl of 10 mM biotin was injected into the brain while 470 nm light (5 mW cm^{-2}, 10 ms pulses at 10 Hz) was delivered for 1.5 h. Whole-tissue lysate analyzed by streptavidin and anti-V5 blotting. The * indicates endogenously biotinylated proteins. This experiment was performed twice with similar results.

(Fig. 2d). In the cytosol, LOV-Turbo was more active than TurboID, whereas TurboID activity was higher in the nucleus and mitochondrial matrix (Fig. 2e).

We found that LOV-Turbo was much less active in the ER lumen and on the surface of HEK 293T cells (Supplementary Fig. 2h–j), which contrasts with its activity on the yeast cell surface, where we performed our directed evolution. We speculated that the oxidative environment of the ER lumen could potentially lead to intra- or intermolecular disulfide formation that disrupts TurboID folding and/or activity. We therefore tested mutation of Cys103 in TurboID or Cys128 in the LOV domain, however, neither Cys removals restored activity in the ER (Supplementary Fig. 2j).

LOV-Turbo is reversible and works in multiple cell types

To test if light-activated LOV-Turbo can reverse to the inactive state when light is removed, we compared biotinylation activity by LOV-Turbo when light is supplied for 15 min and then turned off, versus when light is continually on for 1 h. If LOV-Turbo turns on but then does not reverse when the light is removed, then labeling will continue in the presence of biotin even after the 15-minute light window. Figure 3a shows that this does not occur. We further probed the kinetics of LOV-Turbo turn-on and turn-off in HEK 293T cells (Supplementary Fig. 3a,b). To study turn-on, during a 5-minute light stimulation window, we supplied biotin at the 0-, 1-, 2- or 3-minute mark. The biotinylation intensity progressively decreased, indicating that LOV-Turbo turns on within a minute of light application, consistent with the reported LOV k_{on} of 2 ms (ref. 17) (Supplementary Fig. 3a). To probe turn-off kinetics, we provided light, followed by biotin 0 or 1 min later (Supplementary Fig. 3b). Our results indicate that LOV-Turbo is reversible, and turn-on and turn-off are both fast, occurring within seconds of light application and light removal.

Finally, we tested whether LOV-Turbo can be used for light-dependent proximity labeling in other cell types and in vivo (Fig. 3b–e).

We expressed LOV-Turbo in the cytosol of either bacterial or yeast cells, and performed 4 and 6 h of labeling, respectively, in the presence of blue light and 100 µM biotin. Promiscuous biotinylation was observed in both contexts, with activity comparable to TurboID and miniTurbo, while negligible labeling was observed in omit-light controls (Fig. 3b,c). LOV-Turbo was also active in cultured rat cortical neurons, although a fair comparison to TurboID could not be performed due to the high level of biotin in the culture media, which made it impossible to control the TurboID labeling time window (Fig. 3d and Supplementary Fig. 3c). Last, we tested LOV-Turbo activity in the intact mouse brain (Fig. 3e). Adeno-associated virus containing the LOV-Turbo gene was injected into the primary motor cortex of adult mice and, 2 weeks later, we delivered blue 470 nm light via an implanted optical fiber for 1.5 h while biotin was simultaneously injected into the brain. Promiscuous labeling of endogenous proteins was observed, but not in the omit-light controls. These studies illustrate the versatility of LOV-Turbo across multiple organelles and cell types.

Applications enabled by LOV-Turbo

LOV-Turbo improves the temporal specificity of proximity labeling. In many settings, TurboID can use the low levels of biotin present in culture media or in vivo to initiate labeling before the addition of exogenous biotin. By contrast, LOV-Turbo gives negligible labeling, even in the presence of 0.5 mM biotin, if the light is not supplied (Supplementary Fig. 2d). This difference is particularly pronounced in biotin-rich neuron culture, where TurboID samples show the same level of streptavidin or neutravidin staining whether or not exogenous biotin is added (Fig. 3d and Supplementary Fig. 3c). Furthermore, when targeted to the mitochondria, the ongoing biotinylation activity of TurboID leads to auto-labeling of a critical lysine residue in the targeting sequence, causing mislocalization of the construct to the nucleus and catalysis of background biotinylation of nuclear proteins (Fig. 4a). By contrast, LOV-Turbo in the same context is correctly targeted and produces mitochondria-specific biotinylation. The improvement in mitochondria-specific biotinylation can be observed in HEK 293T cell cultures as well (Supplementary Fig. 3d), although some mistargeting is seen at high expression levels, perhaps due to the larger size and tightly folded structure of LOV-Turbo.

To demonstrate spatial control of proximity labeling with LOV-Turbo, we illuminated a cell culture dish that was partially covered with black tape. Streptavidin staining was observed exclusively in the noncovered, illuminated regions of the sample (Fig. 4b).

A third application enabled by LOV-Turbo is pulse-chase labeling. TurboID labeling can be inhibited by cooling samples to 4 °C (ref. 5), but if cells are maintained at 30 or 37 °C, biotin washout is not sufficient to terminate labeling (Supplementary Fig. 3e). Because LOV-Turbo is turned on reversibly by light (Fig. 3a), the mere removal of light terminates biotinylation. Cells can then continue to be cultured as the LOV-Turbo-labeled proteome redistributes. We demonstrated this in Fig. 4c by performing 10 min of biotinylation with LOV-Turbo, then chasing for 8 h in the dark. A small but noticeable population of biotinylated proteins can be observed in the cytosol after chasing for 8 h but not immediately following biotinylation (Fig. 4c and Supplementary Fig. 3f,g).

Pulse-chase labeling with LOV-Turbo can be combined with organelle fractionation to query biotinylated proteins that have been redistributed into a specific organelle. We demonstrated this by labeling the cytosolic proteome of HEK 293T cells with LOV-Turbo-NES, heat shocking the cells, chasing for 2 h in the dark, then performing nuclear fractionation and streptavidin enrichment to isolate biotinylated proteins in the nucleus (Fig. 4d,e). Figure 4e shows a range of proteins captured by this method, including importin-α and HSP70, which are both known to translocate from the cytosol to the nucleus on heat shock[18,19].

The fourth application of LOV-Turbo we explored is inspired by our previous observation that LOV-based optogenetic tools can be controlled by bioluminescence from luciferases via bioluminescence resonance energy transfer (BRET)[20] (Fig. 4f). We first tested whether LOV-Turbo could be activated by BRET rather than exogenous blue light by directly fusing the 460 nm-emitting luciferase NanoLuc[21] to LOV-Turbo. We observed biotinylation by this construct in HEK 293T cells when NanoLuc's substrate, furimazine, was supplied together with biotin for 10 min or 1 h in the dark (Fig. 4g). Next, we tested an intermolecular BRET configuration by fusing NanoLuc to the GPCR CCR6 and LOV-Turbo to arrestin, which is recruited to CCR6 on activation by CCR6's peptide agonist CCL20 (ref. 22) (Fig. 4h). Figure 4i shows promiscuous biotinylation by arrestin-LOV-Turbo in the presence of furimazine and biotin, in cells treated with the CCL20 agonist but not in untreated cells. Controls omitting furimazine or biotin showed a lack of labeling. These results indicate that it may be possible to use LOV-Turbo and NanoLuc in combination to label the interactomes of defined protein subcomplexes in living cells.

Mapping proteome dynamics with LOV-Turbo by mass spectrometry

We further explored the use of LOV-Turbo for pulse-chase labeling in living cells by performing two quantitative liquid chromatography–tandem mass spectrometry (LC–MS/MS)-based proteomics experiments (Fig. 5a,c). In both, we first used LOV-Turbo to tag the endogenous ER membrane (ERM)-associated proteome from the cytosolic face. We then performed either nuclear fractionation or mitochondrial fractionation, after a chase period of several hours. In both experiments, we analyzed basal trafficking in addition to trafficking following ER stress. Treatment with either tunicamycin[23] (for ER to nucleus) or thapsigargin[24] (for ER to mitochondria) induced ER stress by inhibiting N-linked glycosylation or blocking sarco or ER Ca^{2+}-ATPase, respectively.

Fig. 4 | Applications of LOV-Turbo. a, Reduced background and improved spatial precision with mito-LOV-Turbo in cultured rat cortical neurons. LOV-Turbo or TurboID targeted to the mitochondrial matrix were expressed in cultured rat cortical neurons via AAV1/2 transduction at DIV 6. At DIV 12, neurons were treated with biotin and light for 2 h, then fixed and stained with anti-V5 antibody to detect enzyme expression, and neutravidin-AF647 to detect biotinylated proteins. Scale bar, 10 µm. This experiment was performed once. **b**, Spatial control of proximity labeling with LOV-Turbo. HEK 293T cells expressing cytosolic LOV-Turbo were labeled with biotin and light for 5 min, while half of the sample was covered with black tape. Images show neutravidin staining in lit area only. DIC, differential interference contrast. Scale bar, 500 µm. This experiment was performed once. **c**, Pulse-chase labeling with LOV-Turbo. HEK 293T cells expressing nuclear LOV-Turbo were labeled with biotin and light for 10 min, then chased for 8 h in the dark (other chase times shown in Supplementary Fig. 3g). Images show neutravidin staining before and after the chase period. Arrows point to biotinylated proteins in the cytosol. Scale bar, 10 µm. This experiment was performed once. **d**, Pulse-chase labeling with cytosolic LOV-Turbo following heat shock. After a 2-hour chase at 37 or 42 °C, biotinylated proteins were enriched from purified nuclei. **e**, Blots showing importin-α and HSP70 from the cytosol detected in the nucleus following heat shock. WCL, whole-cell lysate. Nuc, nuclear fraction. SA, streptavidin. This experiment was performed once. **f**, Schematic of BRET-based activation of LOV-Turbo with the luciferase NanoLuc. **g**, Testing a direct fusion of NanoLuc to LOV-Turbo. Addition of NanoLuc's substrate, furimazine, in the dark is sufficient to activate LOV-Turbo and produce promiscuous biotinylation in the cytosol of HEK 293T cells. This experiment was performed twice with similar results. **h**, Schematic of LOV-Turbo activation via arrestin recruitment to activated GPCR-NanoLuc fusion. **i**, Specific proximity labeling by a GPCR-arrestin complex, via BRET-induced LOV-Turbo activation. Arrestin-LOV-Turbo and CCR6-NanoLuc were expressed in HEK 293T cells, and the GPCR (CCR6) was stimulated by its peptide agonist CCL20. Labeling was performed for 1 h in the presence of biotin and furimazine. Anti-Myc detects arrestin-LOV-Turbo expression, and anti-V5 detects CCR6-NanoLuc expression. This experiment was performed three times with similar results.

https://doi.org/10.1038/s41592-023-01880-5

We first used western blotting to check the quality of our organelle-fractionated, streptavidin-enriched material. In our ER-to-nucleus sample, we detected ATF6, a known stress-responsive ER-localized transcription factor[25] (Supplementary Fig. 4a). In agreement with literature[25,26], we found that nuclear ATF6 is cleaved after tunicamycin-induced ER stress. Supplementary Fig. 5a shows the population of proteins detected in our ER-to-mitochondria sample. Encouragingly, treatment of cells with FCCP (carbonyl cyanide *p*-(trifluoromethoxy)phenylhydrazone), which depolarizes mitochondria and prevents protein import, reduced the quantity of proteins remaining after mitochondrial fractionation and streptavidin enrichment.

The design of our ER-to-nucleus proteomic experiment is shown in Supplementary Fig. 4c. Negative controls omitting light or the 2-hour chase, spatial references with cytosolic LOV-Turbo and whole-cell lysate were included in the 18-plex tandem mass tag (TMT) labeling experiment. A total of 5,308 proteins were detected and quantified LC–MS/MS with good correlation observed between replicates (Supplementary Fig. 4d). To check the specificity of the data, we plotted enrichment ratios (experiment versus omit light, experiment versus cytosolic reference and so on) as receiver operating characteristic curves, using known ER or nuclear proteins as true positives and known mitochondrial proteins as false positives (Supplementary Fig. 4e–g). We observed that ER and nuclear proteins were strongly enriched over

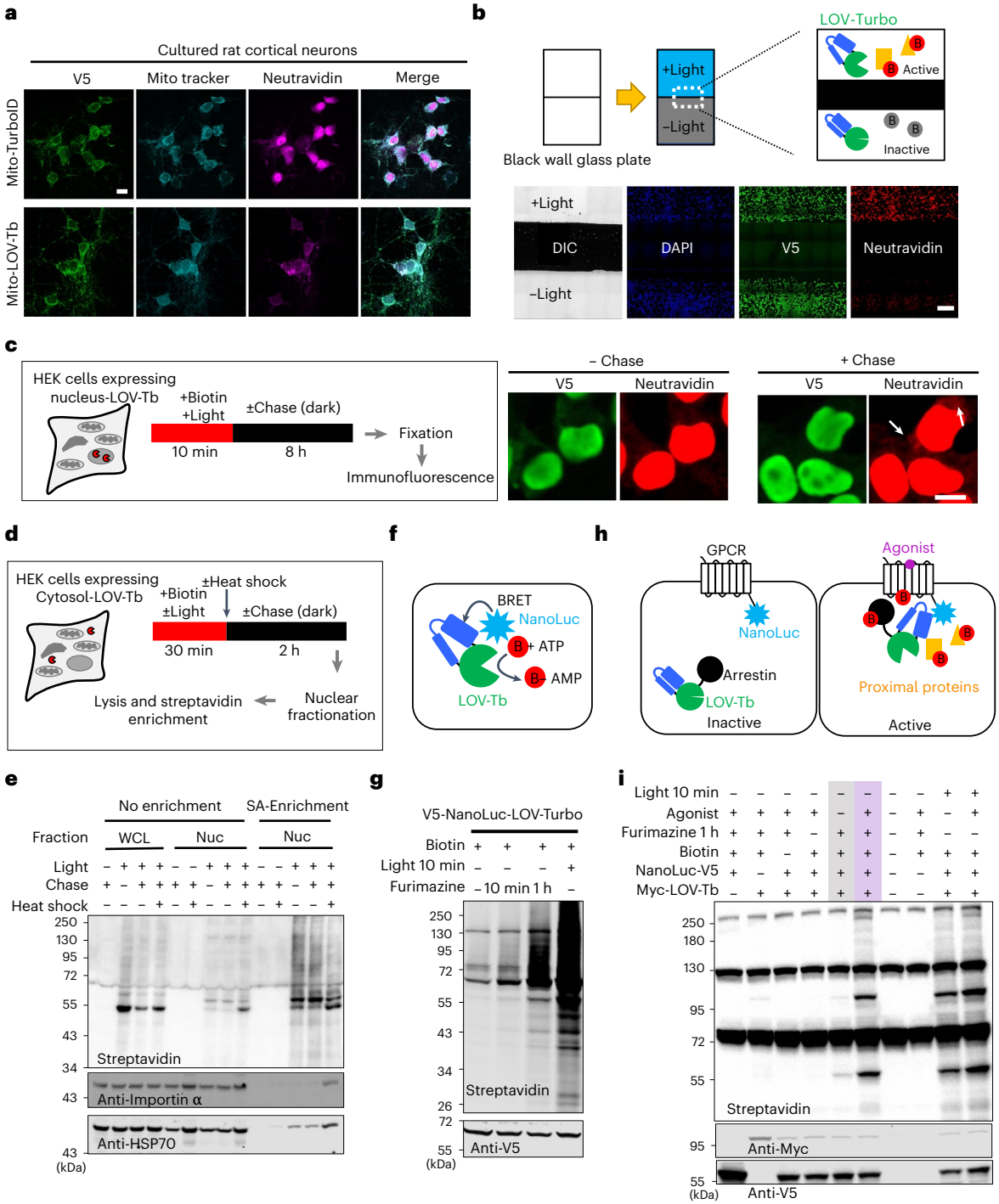

https://doi.org/10.1038/s41592-023-01880-5

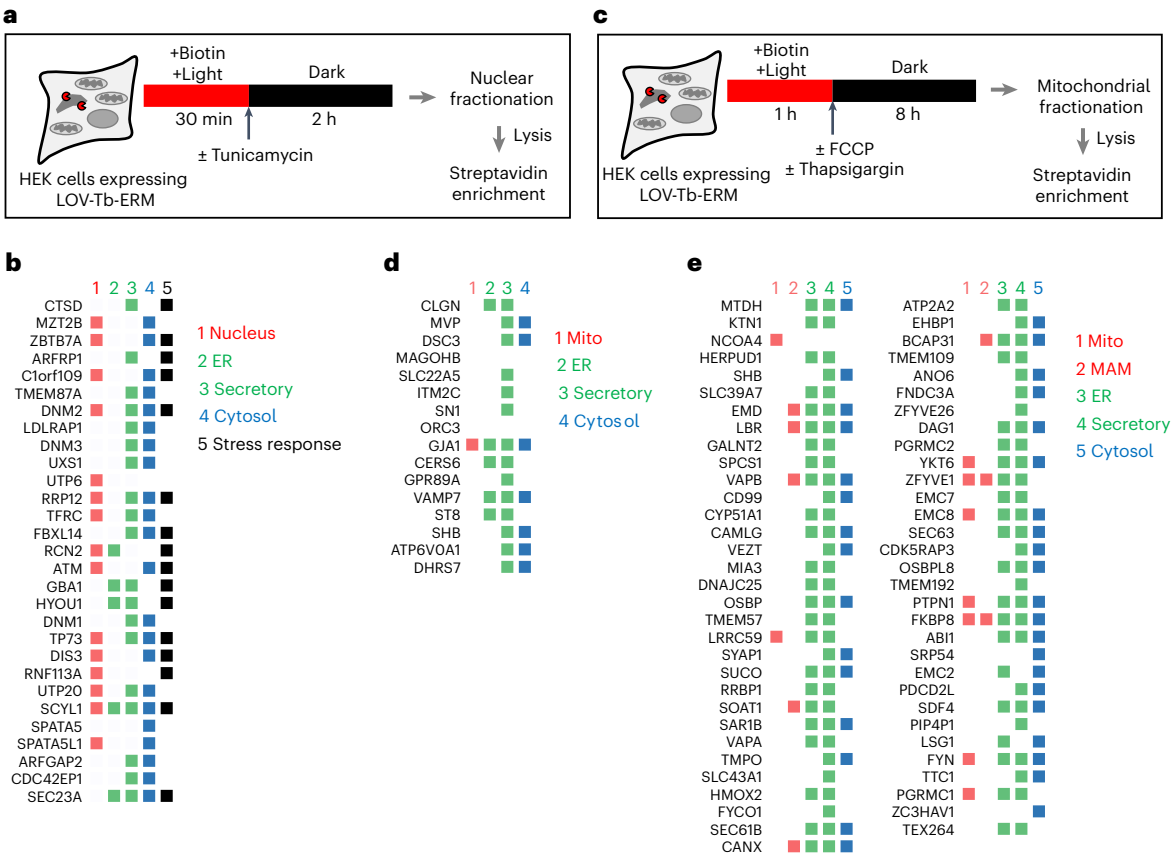

Fig. 5 | Mapping proteome dynamics with LOV-Turbo by mass spectrometry. **a**, Scheme for pulse-chase labeling with LOV-Turbo localized to the ERM facing the cytosol. After a 2-hour chase, biotinylated proteins were enriched from purified nuclei. See Supplementary Fig. 4c for design of 18-plex proteomic experiment. **b**, 29 proteins that exhibit increased trafficking from ERM to nucleus following stress induction by tunicamycin. Proteins are ranked by fold-change compared to basal (no stress) condition. Colorings based on GOCC annotation (details in Supplementary Table 2). **c**, Scheme for pulse-chase labeling with LOV-Turbo at the ERM facing the cytosol. After an 8-h chase, biotinylated proteins are enriched from purified mitochondria. See Supplementary Fig. 5b for design of 17-plex proteomic experiment. **d**, 16 proteins detected in ERM to mitochondria dataset from **c** under basal conditions. Proteins ranked by fold-change compared to FCCP control, which inhibits mitochondrial protein import. Coloring reflects GOCC annotations (details in Supplementary Table 3). **e**, 63 proteins that exhibit increased trafficking from ERM to mitochondria following thapsigargin treatment. Proteins ranked by fold-change compared to basal condition. Colorings based on GOCC annotation (details in Supplementary Table 3). MAM, mitochondria-associated membranes, which includes mitochondria-ER contact site proteins.

mitochondrial proteins with high TMT ratios, helping to confirm the specificity of our dataset.

As shown in Supplementary Fig. 4h, the 5,308 detected proteins were filtered by *P* value and fold-change with respect to omit-light, omit-tunicamycin, cytosolic LOV-Turbo and whole-cell lysate samples, to obtain a final list of 29 proteins that show increased ER-to-nucleus trafficking after tunicamycin treatment (Supplementary Table 2). Within this list, 20 proteins have secretory pathway annotation, 15 proteins have nuclear annotation and seven have both nuclear and secretory annotation (Fig. 5b). Out of 29 proteins, 16 are known stress-responsive proteins. Three of our hits have previously been reported to translocate to the nucleus under stress (Serine-protein kinase ATM[27], Cathepsin D CTSD[28] and Hypoxia upregulated protein 1 HYOU1, ref. 29). Especially, ATM is an ER stress-responsive protein[30], although the localization is still controversial[31]. Our dataset also may contain potential artifacts, such as nuclear proteins that are translated by ER-associated ribosomes during the biotinylation time window (for example, nucleolar protein UTP6).

Nevertheless, we were intrigued by N-terminal kinase-like protein SCYL1. This protein has both ER or Golgi annotation[32] and nuclear annotation, as one of its isoforms may bind to the human TERT promoter[33]. Reticulocalbin-2 RCN2 also appears in our dataset. It is ER-annotated by Gene Ontology Cellular Component (GOCC)[34,35], and enriched in our previous ERM-APEX2 dataset[36]. Although its function is unknown, previous studies have shown that RCN2 levels decrease after thapsigargin treatment in Huh7 cells[37]. See Supplementary Note 1 for further analysis of this dataset.

In our second proteomic experiment, we combined LOV-Turbo labeling at the ERM with mitochondrial fractionation. The design of the 17-plex proteomic experiment is shown in Supplementary Fig. 5b, incorporating controls omitting light or inhibiting mitochondrial protein import with FCCP. 5107 proteins were detected by LC–MS/MS with good correlation between replicates (Supplementary Fig. 5c), and we performed filtering as shown in Supplementary Fig. 5e. The receiver operating characteristic curves in Supplementary Fig. 5d show strong enrichment of ER-annotated true positive proteins over false positive nuclear proteins, in both basal and thapsigargin-treated datasets. After filtering, we obtained lists of 16 and 64 proteins that traffic from ER to mitochondria under basal and thapsigargin stress conditions, respectively. (Supplementary table 3)

Both lists are enriched in ER and secretory pathway-annotated proteins (Fig. 5d,e). We identified a number of proteins associated with mitochondria-ER contact sites, as our filtering procedure does not eliminate such proteins; these include EMD[38], LBR[38], VAPB[38], SOAT1

(ref. 38), BCAP31 (ref. 38), FKBP8 (ref. 38), CANX (ref. 39) and ZFYVE1 (ref. 39). We also observed some artifacts likely resulting from contamination of mitochondrial fractions with ER-derived vesicles (for example, the ER transmembrane proteins MTDH, KTN1, HERPUD1). We were intrigued by the tyrosine-protein phosphatase PTPN1, found in our thapsigargin dataset. Annotated as both a peripheral ERM protein and a mitochondrial matrix protein by GOCC, PTPN1 is activated under ER stress and serves as a negative regulator for insulin and leptin signaling[40,41]. It also modulates oxidative phosphorylation, and its inhibition has been shown to promote mitochondrial fusion[42]. If PTPN1 shuttles from the ERM into mitochondria on stress, as suggested by our LOV-Turbo pulse-chase labeling, this could serve as a mechanism to coordinate the ER stress response with mitochondrial oxidative phosphorylation and/or mitochondrial dynamics.

Discussion

Through a combination of structure-guided design, screening and directed evolution, we have developed a reversible blue light-gated variant of the proximity labeling enzyme TurboID. LOV-Turbo is 50 kDa, roughly 16 kDa larger than TurboID (34 kDa) and boasts an extremely wide dynamic range: activity is virtually undetectable in the dark state, even in the presence of 0.5 mM biotin (50–100 µM biotin is typically used for labeling) and light-state activity is comparable to TurboID. In this study, fold turn-ons of LOV-Turbo ranged from 50- to 170-fold, depending on labeling time and organelle. Light-induced turn-on is rapid and can be rapidly reversed as well by simply removing the light source. We showed that LOV-Turbo works in multiple mammalian subcompartments, in yeast and bacteria, and also in the mouse brain.

A common strategy for introducing light gating to engineered proteins is to split the protein into fragments, and attach the fragments to light-inducible dimerizing proteins such as CRY/CIBN[43] or FKF1/GI (ref. 44). Such an approach has been used to produce light-gated versions of transcription activator-like effectors[45], botulinum toxin[46] and Gal4 (ref. 47). However, such tools are more cumbersome to use, as two separate components must be introduced, and tool performance varies depending on expression ratio as well as absolute expression level: with low reconstitution and/or signal at low expression levels and possible false positives or light-independent background at high expression levels. Although we have previously developed split-TurboID[38], we opted not to use it as the basis of light-gated TurboID. Instead, we aimed for a single, compact construct that would be simpler to use and work robustly across a range of expression levels.

Several studies have engineered allosteric regulation by small molecules or light into proteins of interest, most commonly transcription factors[45,48]. There are fewer examples of engineered allosteric regulation of enzymes[2–4]. In our own previous work[3], we introduced calcium-binding domains into a distal surface-exposed loop of tobacco etch virus protease to produce a Ca^{+2}-activated protease that was used in a transcriptional Ca^{+2} integrator tool called scFLARE. Here we show that this approach is more broadly applicable. Some screening is required to identify a sensitive site for the insertion of protein domains that are conformationally responsive to analytes or light. Examination of the AlphaFold-predicted structure of LOV-Turbo (Fig. 2a) suggests that the 80/81 loop works because it is connected by a beta-strand to the biotin-binding pocket of TurboID. The 'clamped' form of the hLOV1 domain in the dark state may distort TurboID's biotin-binding pocket just enough to prevent substrate binding, while light releases the clamp and restores TurboID's structure to a native-like conformation. Future structural and kinetic analyses of LOV-Turbo may reveal the structural features and enzymatic substeps that are most influenced by light.

A recent report described photo-Turbo, a different light-gated version of TurboID[49]. With a nitrobenzyl-caged catalytic lysine, introduced by unnatural amino acid mutagenesis. Photo-Turbo is much more complicated to use due to the need for unnatural amino acid incorporation, not genetically encoded and not reversible. Uncaging also requires 365 nm ultraviolet light, which can be phototoxic. More recently, a few reports have described light-catalyzed proximity labeling using mutants of the LOV domain (LOV*)[50,51]. High power (30–450 mW cm^{-2}) blue light is used to induce singlet oxygen generation by LOV*, which in turn produces biotin-phenoxyl radicals for labeling. Our LOV-Turbo requires far weaker light for activation (roughly 1 mW cm^{-2}), no special media and labeling is performed with biotin, which is easier to deliver to cells, tissues and animals than biotin-phenol. The low power requirement of LOV-Turbo enables the luciferase/BRET-based turn-on shown in Fig. 4f–i, which we do not believe would be possible with LOV*.

We have demonstrated several applications of LOV-Turbo, capitalizing on the improved temporal and spatial control afforded by light gating. LOV-Turbo suppressed background labeling before exogenous biotin addition that can plague TurboID experiments, especially in vivo. We used the reversible light regulation of LOV-Turbo to perform pulse-chase proteomics, identifying proteins that may shuttle between the ER and nucleus or mitochondria under normal and stressed conditions. Finally, we showed that instead of external blue light, LOV-Turbo can be activated by the luciferase NanoLuc via BRET, enabling us to selectively biotinylate protein subcomplexes, defined by proximity between a LOV-Turbo-fusion protein and a NanoLuc-fused protein.

It is also important to note LOV-Turbo's limitations. Unlike TurboID, LOV-Turbo is inactive in the secretory compartment of mammalian cells. It also displays inferior targeting to some compartments such as the mitochondrial matrix, perhaps a result of its larger size and the high stability of the hLOV domain. Finally, further engineering will be required to improve the efficiency of BRET-based activation of LOV-Turbo by NanoLuc before this approach can be widely applied for subcomplex-specific proteome mapping.

Online content

Any methods, additional references, Nature Portfolio reporting summaries, source data, extended data, supplementary information, acknowledgements, peer review information; details of author contributions and competing interests; and statements of data and code availability are available at https://doi.org/10.1038/s41592-023-01880-5.

References

1. Bruder, M., Polo, G. & Trivella, D. B. B. Natural allosteric modulators and their biological targets: molecular signatures and mechanisms. *Nat. Prod. Rep.* **37**, 488–514 (2020).
2. Wu, Y. I. et al. A genetically encoded photoactivatable Rac controls the motility of living cells. *Nature* **461**, 104–108 (2009).
3. Sanchez, M. I., Nguyen, Q.-A., Wang, W., Soltesz, I. & Ting, A. Y. Transcriptional readout of neuronal activity via an engineered Ca^{2+}-activated protease. *Proc. Natl Acad. Sci. USA* **117**, 33186–33196 (2020).
4. Kimberly, R. & Ranganathan, R. Hot spots for allosteric regulation on protein surfaces. *Cell* **147**, 1564–1575 (2011).
5. Branon, T. C. et al. Efficient proximity labeling in living cells and organisms with TurboID. *Nat. Biotechnol.* **36**, 880–887 (2018).
6. Qin, W., Cho, K. F., Cavanagh, P. E. & Ting, A. Y. Deciphering molecular interactions by proximity labeling. *Nat. Methods* **18**, 133–143 (2021).
7. Cho, K. F. et al. Proximity labeling in mammalian cells with TurboID and split-TurboID. *Nat. Protoc.* **15**, 3971–3999 (2020).
8. Wood, Z. A., Weaver, L. H., Brown, P. H., Beckett, D. & Matthews, B. W. Co-repressor induced order and biotin repressor dimerization: a case for divergent followed by convergent evolution. *J. Mol. Biol.* **357**, 509–523 (2006).
9. Kim, M. W. et al. Time-gated detection of protein-protein interactions with transcriptional readout. *eLife* **6**, e30233 (2017).
10. Kim, C. K. et al. A molecular calcium integrator reveals a striatal cell type driving aversion. *Cell* **183**, 2003–2019.e2016 (2020).

11. Lam, S. S. et al. Directed evolution of APEX2 for electron microscopy and proximity labeling. *Nat. Methods* **12**, 51–54 (2015).
12. Jumper, J. et al. Highly accurate protein structure prediction with AlphaFold. *Nature* **596**, 583–589 (2021).
13. Guntas, G. et al. Engineering an improved light-induced dimer (iLID) for controlling the localization and activity of signaling proteins. *Proc. Natl Acad. Sci. USA* **112**, 112–117 (2015).
14. Lee, D. et al. Temporally precise labeling and control of neuromodulatory circuits in the mammalian brain. *Nat. Methods* **14**, 495–503 (2017).
15. Kawano, F., Aono, Y., Suzuki, H. & Sato, M. Fluorescence imaging-based high-throughput screening of fast- and slow-cycling LOV proteins. *PLoS ONE* **8**, e82693 (2013).
16. Wang, W. et al. A light- and calcium-gated transcription factor for imaging and manipulating activated neurons. *Nat. Biotechnol.* **35**, 864–871 (2017).
17. Eitoku, T., Nakasone, Y., Matsuoka, D., Tokutomi, S. & Terazima, M. Conformational dynamics of phototropin 2 LOV2 domain with the linker upon photoexcitation. *J. Am. Chem. Soc.* **127**, 13238–13244 (2005).
18. Welch, W. J. & Feramisco, J. R. Nuclear and nucleolar localization of the 72,000-dalton heat shock protein in heat-shocked mammalian cells. *J. Biol. Chem.* **259**, 4501–4513 (1984).
19. Miyamoto, Y. et al. Cellular stresses induce the nuclear accumulation of importin α and cause a conventional nuclear import block. *J. Cell Biol.* **165**, 617–623 (2004).
20. Kim, C. K., Cho, K. F., Kim, M. W. & Ting, A. Y. Luciferase-LOV BRET enables versatile and specific transcriptional readout of cellular protein-protein interactions. *eLife* **8**, e43826 (2019).
21. Hall, M. P. et al. Engineered Luciferase reporter from a deep sea shrimp utilizing a novel imidazopyrazinone substrate. *Am. Chem. Soc. Chem. Biol.* **7**, 1848–1857 (2012).
22. Hedrick, M. N., Lonsdorf, A. S., Hwang, S. T. & Farber, J. M. CCR6 as a possible therapeutic target in psoriasis. *Expert Opin. Ther. Targets* **14**, 911–922 (2010).
23. Olden, K., Pratt, R. M., Jaworski, C. & Yamada, K. M. Evidence for role of glycoprotein carbohydrates in membrane transport: specific inhibition by tunicamycin. *Proc. Natl Acad. Sci. USA* **76**, 791–795 (1979).
24. Lytton, J., Westlin, M. & Hanley, M. R. Thapsigargin inhibits the sarcoplasmic or endoplasmic reticulum Ca-ATPase family of calcium pumps. *J. Biol. Chem.* **266**, 17067–17071 (1991).
25. Haze, K., Yoshida, H., Yanagi, H., Yura, T. & Mori, K. Mammalian transcription factor ATF6 is synthesized as a transmembrane protein and activated by proteolysis in response to endoplasmic reticulum stress. *Mol. Biol. Cell* **10**, 3787–3799 (1999).
26. Ye, J. et al. ER stress induces cleavage of membrane-bound ATF6 by the same proteases that process SREBPs. *Mol. Cell* **6**, 1355–1364 (2000).
27. Berthel, E., Foray, N. & Ferlazzo, M. L. The nucleoshuttling of the ATM protein: a unified model to describe the individual response to high- and low-dose of radiation? *Cancers* **11**, 905 (2019).
28. Zhao, S., Aviles, E. R. Jr & Fujikawa, D. G. Nuclear translocation of mitochondrial cytochrome c, lysosomal cathepsins B and D, and three other death-promoting proteins within the first 60 minutes of generalized seizures. *J. Neurosci. Res.* **88**, 1727–1737 (2010).
29. Billing, A. M. et al. Proteomic profiling of rapid non-genomic and concomitant genomic effects of acute restraint stress on rat thymocytes. *J. Proteom.* **75**, 2064–2079 (2012).
30. Hotokezaka, Y., Katayama, I. & Nakamura, T. ATM-associated signalling triggers the unfolded protein response and cell death in response to stress. *Commun. Biol.* **3**, 378 (2020).
31. Lee, J.-H. & Paull, T. T. Mitochondria at the crossroads of ATM-mediated stress signaling and regulation of reactive oxygen species. *Redox Biol.* **32**, 101511 (2020).
32. Burman, J. L. et al. Scyl1, mutated in a recessive form of spinocerebellar neurodegeneration, regulates COPI-mediated retrograde traffic. *J. Biol. Chem.* **283**, 22774–22786 (2008).
33. Tang, Z. et al. Molecular cloning and characterization of a human gene involved in transcriptional regulation of hTERT. *Biochem. Biophys. Res. Commun.* **324**, 1324–1332 (2004).
34. Ashburner, M. et al. Gene ontology: tool for the unification of biology. The Gene Ontology Consortium. *Nat. Genet.* **25**, 25–29 (2000).
35. Gene Ontology Consortium. The Gene Ontology resource: enriching a GOld mine. *Nucleic Acids Res.* **49**, D325–d334 (2021).
36. Hung, V. et al. Proteomic mapping of cytosol-facing outer mitochondrial and ER membranes in living human cells by proximity biotinylation. *eLife* **6**, e24463 (2017).
37. Amodio, G. et al. Proteomic signatures in thapsigargin-treated hepatoma cells. *Chem. Res. Toxicol.* **24**, 1215–1222 (2011).
38. Cho, K. F. et al. Split-TurboID enables contact-dependent proximity labeling in cells. *Proc. Natl Acad. Sci. USA* **117**, 12143–12154 (2020).
39. Hamasaki, M. et al. Autophagosomes form at ER–mitochondria contact sites. *Nature* **495**, 389–393 (2013).
40. Zabolotny, J. M. et al. PTP1B regulates leptin signal transduction in vivo. *Dev. Cell* **2**, 489–495 (2002).
41. Galic, S. et al. Coordinated regulation of insulin signaling by the protein tyrosine phosphatases PTP1B and TCPTP. *Mol. Cell. Biol.* **25**, 819–829 (2005).
42. Kornicka-Garbowska, K., Bourebaba, L., Röcken, M. & Marycz, K. Inhibition of protein tyrosine phosphatase improves mitochondrial bioenergetics and dynamics, reduces oxidative stress, and enhances adipogenic differentiation potential in metabolically impaired progenitor stem cells. *Cell Commun. Signal.* **19**, 106 (2021).
43. Kennedy, M. J. et al. Rapid blue-light–mediated induction of protein interactions in living cells. *Nat. Methods* **7**, 973–975 (2010).
44. Kim, W.-Y. et al. ZEITLUPE is a circadian photoreceptor stabilized by GIGANTEA in blue light. *Nature* **449**, 356–360 (2007).
45. Konermann, S. et al. Optical control of mammalian endogenous transcription and epigenetic states. *Nature* **500**, 472–476 (2013).
46. Liu, Q. et al. A photoactivatable botulinum neurotoxin for inducible control of neurotransmission. *Neuron* **101**, 863–875. e866 (2019).
47. Yazawa, M., Sadaghiani, A. M., Hsueh, B. & Dolmetsch, R. E. Induction of protein-protein interactions in live cells using light. *Nat. Biotechnol.* **27**, 941–945 (2009).
48. Polstein, L. R. & Gersbach, C. A. A light-inducible CRISPR-Cas9 system for control of endogenous gene activation. *Nat. Chem. Biol.* **11**, 198–200 (2015).
49. Liu, Y. et al. Spatiotemporally resolved subcellular phospho-proteomics. *Proc. Natl Acad. Sci. USA* **118**, e2025299118 (2021).
50. Hananya, N., Ye, X., Koren, S. & Muir, T. W. A genetically encoded photoproximity labeling approach for mapping protein territories. *Proc. Natl Acad. Sci. USA* **120**, e2219339120 (2023).
51. Zhai, Y. et al. Spatiotemporal-resolved protein networks profiling with photoactivation dependent proximity labeling. *Nat. Commun.* **13**, 4906 (2022).

Publisher's note Springer Nature remains neutral with regard to jurisdictional claims in published maps and institutional affiliations.

Springer Nature or its licensor (e.g. a society or other partner) holds exclusive rights to this article under a publishing agreement with the author(s) or other rightsholder(s); author self-archiving of the accepted manuscript version of this article is solely governed by the terms of such publishing agreement and applicable law.

© The Author(s), under exclusive licence to Springer Nature America, Inc. 2023

Methods

Labeling in mammalian cells with LOV-Turbo

HEK 293T cells transiently or stably expressing LOV-Turbo or its variants under a pTRE3G promoter were induced with 100–200 ng ml^{-1} doxycycline overnight. After induction, cells were covered with aluminum foil until ready for blue light stimulation. When uncovered, cells were handled in a dark room with red light illumination to avoid undesired activation of LOV-Turbo. To stimulate LOV-Turbo, biotin was added to cell cultures to a final concentration of 100 µM (unless noted otherwise) and incubated at 37 °C while being placed directly on top of a blue light light-emitting diode (LED) array. We used an AMUZA system consisting of a blue LED array, an LED Array Driver and pulse generator. We used a 10% duty cycle, 10 ms on and 90 ms off, for 30 min unless noted otherwise. Light power before pulse generation was typically around 10 mW cm^{-2} (measured by Thorlabs PM100D), unless noted otherwise. As shown in Fig. 2b, continuous blue light at 1 mW cm^{-2} activates LOV-Turbo just as well. Alternatively, 10 ms to 1 s pulses of 2.5 mW cm^{-2} light at a 33% duty cycle give a comparable degree of activation, as shown in Supplementary Fig. 2g. Note that we used 12-well cell culture plates (Corning, no. 3513) to test required light power, which may vary in thickness across different plate manufacturers. Control samples were processed in parallel omitting light or biotin. Following light stimulation, cells were once again handled under red light, washed in ice-cold Dulbecco's PBS (DPBS) three times and analyzed by western blot or immunofluorescence as described below.

Western blot detection of LOV-Turbo activity

Following light stimulation, cells were washed in cold DPBS three times and lysed directly in the cell culture wells with RIPA lysis buffer supplemented with 1× protease inhibitor cocktail (Sigma-Aldrich). Lysates were cleared via centrifugation at 20,000*g* at 4 °C for 10 min. Cleared lysates were mixed with protein loading buffer and boiled at 95 °C for 5 min. Samples were then loaded on 10% SDS–PAGE gels, transferred onto nitrocellulose membrane, and stained with Ponceau S (Sigma) to visualize total protein loading. Blots were blocked in 5% (w/v) nonfat milk (Lab Scientific, M-0841) in 1× tris-buffered saline with Tween (TBST) (Teknova) for 30–60 min at room temperature, incubated with mouse anti-V5 primary antibody against LOV-Turbo's epitope tag in TBST for 1 h at room temperature, washed three times with TBST for 5 min each, incubated in antimouse-IRDye680 secondary antibody and streptavidin-IRDye800 or streptavidin-HRP for 30 min at room temperature, washed three times with TBST and imaged on an Odyssey CLx imager (LICOR) or ChemiDoc XRS+ imager with Clarity Western ECL Blotting Substrates (Bio-Rad). See antibody sources and dilutions used in the Supplementary Information. Quantification of labeling (in Figs. 1b,c,g,h and 2b, and Supplementary Figs. 1g,i, 2c,d,f,g and 3a) was performed with Image Studio (LICOR) except for Fig. 1b, which used ImageJ (NIH), by selecting the entire gel lane and subtracting endogenous biotinylated protein bands.

Immunofluorescence detection of LOV-Turbo activity

Before labeling, cells were plated on glass coverslips coated with 25 µg ml^{-1} human fibronectin in DPBS for 1 h at 37 °C. After LOV-Turbo labeling, cells were fixed with 4% (v/v) paraformaldehyde in DPBS for 15 min, washed three times with DPBS, and permeabilized with ice-cold methanol at 4 °C for 10 min or with 0.1% Triton X-100 in DPBS at room temperature for 10 min. Cells were then washed three times with DPBS and blocked for 1 h with 2% BSA (w/v) in DPBS at room temperature. Samples were incubated with primary antibodies in 1% BSA in TBST for 1–2 h at room temperature. We used anti-V5 antibody to detect LOV-Turbo's epitope tag, antibodies against TOM20 and calnexin to visualize mitochondria and ER, respectively, and other antibodies as listed in the Supplementary Information. Sometimes, we used MitoTracker (Invitrogen, M22426) to visualize mitochondria following the manufacturer's protocol in live cells. After primary antibody incubation, cells were washed three times in TBST and then incubated with secondary antibodies and neutravidin conjugated to AlexaFluor-488/568/647 in 1% BSA in TBST for 1 h at room temperature. Cells were washed three times with TBST and then incubated with 300 nM 4,6-diamidino-2-phenylindole (DAPI) in DPBS for 5 min. Cells were washed three times with DPBS and mounted on glass slides and imaged by confocal fluorescence microscopy (Zeiss). Images were collected with Slidebook (Intelligent Imaging Innovations).

Mammalian cell culture, transfection and generation of stable cell lines

HEK 293T cells (from ATCC, CRL-3216) were cultured in DMEM containing 10% fetal bovine serum, 100 U ml^{-1} penicillin, and streptomycin at 37 °C and 5% CO_2. For transient expression (Figs. 1b,c and 4g and Supplementary Figs. 1b,f–h and 2h–j), cells in 12-well plates were typically transfected at roughly 70% confluency using 2.5 µl of polyethyleneimine (PEI, 1 mg ml^{-1} in water, pH 7.3) or Lipofectamine 2000 (Life Technologies) and a total 1,000 ng of plasmid in 100 µl of serum-free media. Cells were incubated with 1 ml of complete media supplemented with 100–200 ng ml^{-1} doxycycline overnight. Stable cell lines were generated with lentivirus infection. Lentivirus was generated by transfecting HEK 293T cells plated to roughly 60% confluency in a six-well dish with 250 ng of pMD2G, 750 ng of psPAX2 and 1,000 ng of lentiviral vector containing the gene of interest with 10 µl of polyethyleneimine (1 mg ml^{-1} in water, pH 7.3) in serum-free media. Lentivirus-containing supernatant was collected after 48 h and filtered through a 0.45 µm filter. HEK 293T cells at roughly 60% confluency were infected with crude lentivirus followed by selection with 10 µg ml^{-1} puromycin for 1 week. To induce expression of proteins under doxycycline-inducible promoter, cells were incubated with media supplemented with 100–200 ng ml^{-1} doxycycline overnight.

Analysis of LOV-Turbo activity on the yeast surface

Yeast cells expressing surface-displayed LOV-Turbo as Aga2 fusions in a pCTCON2 (ref. 52) vector were cultured overnight in biotin-depleted media (BDM) (Yeast cell culture) to induce expression. Next, 6×10^9 cells (one optical density (OD_{600}) of 1×10^7 cells) were transferred into 1 ml of BDM containing 1 mM ATP, 5 mM $MgCl_2$ and 1–50 µM of biotin. Cultures were then incubated at 30 °C or 37 °C for 1.5 h with or without light exposure, while rotating. To keep samples in the dark, tubes were wrapped in aluminum foil. For light stimulation, samples were exposed to ambient light plus an additional blue light bulb overhead. After biotin labeling, samples were kept on ice to stop the labeling. Yeast cells were washed in cold phosphate-buffered saline (PBS) containing 0.1% BSA (PBS-B) three times by pelleting at 3,000*g* for 2 min at 4 °C and resuspending in 1 ml cold PBS-B. Yeast cells were stained in 50 µl of PBS-B containing anti-Myc antibody (1:400) for 1 h at 4 °C for detecting ligase expression, then the cells were washed three more times and stained in 50 µl of PBS-B with goat antichicken-AF488 or antichicken-AF647 and SA-PE for 40 min at 4 °C. Samples were washed for the final three times with 1 ml PBS-B before analysis or sorting. To analyze and sort, single yeast cells were gated on a forward-scatter area (FSC-A) by side-scatter area (SSC-A) plot around the clustered population (P1) on a ZE5 Cell Analyzer (Bio-Rad). P1 was then gated on a side-scatter width (SSC-W) by side-scatter height (SSC-H) plot around the clustered population (P2). P2 populated cells were then plotted to detect AF488 or AF647 and phycoerythrin signals. FlowJo v10 (BD Biosciences) was used to analyze FACS data. Quantification of biotinylation in Fig. 1f and Supplementary Fig. 1e was calculated as the percentage of yeasts in P2 in the upper quadrants I and III as drawn in Fig. 1f. Quantification of expression in Fig. 1f and Supplementary Fig. 1e was calculated as the percentage of yeasts in P2 in the right-most quadrants III and IV.

Yeast-display library generation

The LOV-Turbo mutant library was generated using error-prone PCR with 100 ng of LOV-Turbo1 as the template. Two libraries were generated

at different levels of mutagenesis under 2 μM 8-oxo-dGTP and either 2 or 1 μM dPTP with 15 PCR cycles following published protocols[53] with the following primers:

F: 5′-ggaggctctggtggaggcggtagcggaggcggagggtcggctagc-3′
R: 5′-gatctcgagctattacaagtcctcttcagaaataagcttttgttcggatcc-3′

PCR products were gel purified then reamplified for 30 more cycles under normal conditions and gel purified again. The pCTCON2 backbone was digested with NheI and BamHI and gel purified as well. Both 4,000 ng of PCR product and 1,000 ng of cut vector were mixed and dried in a DNA speed vacuum (DNA110 Savant). The dried DNA was then resuspended in 10 μl of water and electroporated into electrocompetent EBY100 yeasts. After electroporation, yeasts were rescued in 2 ml of yeast extract peptone dextrose media and recovered at 30 °C without shaking for 1 h. Then, 1.98 ml of the culture was propagated in 100 ml of SDCAA medium while 20 μl was used to determine library size. Yeasts were diluted 100×, 1,000×, 10,000×, 100,000× and 20 μl of each dilution was plated onto SDCAA plates at 30 °C for 3 days. The resulting library size was determined by the number of colonies on the 100×, 100×, 1,000× and 100,000× plates, corresponding to 10^4, 10^5, 10^6 or 10^7 transformants in the library, respectively. The library sizes resulting from the two levels of mutagenic error-prone PCR were 3.4×10^7 and 2.6×10^7. Both libraries were combined in equal volume to form our yeast-display library.

Directed evolution of LOV-Turbo on yeast

The two LOV-Turbo libraries generated above were combined 1:1. For the first round of selection, yeast cells were labeled with 1 μM of biotin for 1.5 h at 30 °C then subsequently processed by staining with primary and secondary antibodies as described above. To sort on a BD FACS Aria II cell sorter (BD Biosciences), gates for singlets were drawn on an FSC-A by SSC-A plot to generate population of one (P1). P1 was then gated on an FSC-A and FSC-H to generate population two (P2), and then P2 was gated on an SSC-A and SSC-W plot to further filter for singlets to generate population 3 (P3). P3 was then gated on a AF647 by SA-PE plot to collect high expressing and high activity clones, as shown in Fig. 1d. In round 1, we collected the top 0.2% of expressing and biotinylated cells, or roughly 5.9×10^5 cells. In rounds 2 and 3, 5.9×10^4 and 2.0×10^4 cells were collected, respectively, making up less than 0.1% of the previously enriched libraries.

Rounds 4 and 5 were negative selections to remove LOV-Turbo mutants with activity in the dark state. Yeast populations were incubated with 50 μM biotin for 4 h in the dark at 30 °C. Rectangular gates were drawn on the bottom right corner of the AF647 by SA-PE plots. Next, 5.0×10^5 (2.5%) and 1.8×10^5 (0.8%) cells were collected, respectively, in rounds 4 and 5. In rounds 6 and 7, we performed positive selection at 37 °C rather than 30 °C, to select for mutants with good expression and stability at this higher temperature (the temperature used for applications in mammalian cells). Yeast cells were incubated with 1 μM biotin for 1.5 h. Rectangular gates were drawn on the top right corner of AF647 by SA-PE plots. Rounds 6 and 7 collected 1.1×10^4 and 1.5×10^3 cells, respectively, making up less than 0.1% of the previously enriched libraries.

Yeast cell culture

Saccharomyces cerevisiae strain EBY100 was propagated at 30 °C in SDCAA media supplemented with 20 mg l^{-1} tryptophan. Competent yeast cells were transformed with yeast-display plasmid pCTCON2 following the Frozen EZ Yeast Transformation II protocol. Successful transformants were selected in SDCAA plates and propagated in SDCAA media. To induce protein expression, yeasts were inoculated from saturated cultures in 10% SD/GCAA (SDCAA with 90% of dextrose replaced with galactose) or BDM (1.7 g l^{-1} YNB-biotin, 5 g l^{-1} ammonium sulfate, 18 g l^{-1} galactose, 2 g l^{-1} dextrose, 5 g l^{-1} casamino acid and 0.5 nM biotin) overnight from a 1:20–1:100 dilution.

LOV-Turbo labeling in the yeast cytosol

To collect western blot samples of BY4741 *S. cerevisiae* in Fig. 3c, competent BY4741 were generated and transformed following the Frozen EZ Yeast Transformation II protocol. Yeast cells were plated on leucine-depleted plates (supplemented minimal medium (SMM) 6.7 g l^{-1} Difco nitrogen base, 20 g l^{-1} dextrose, 0.69 g l^{-1} CSM-Leu (Sunrise Science Products), with 20 g l^{-1} agar) to select for successful transformants at 30 °C. Colonies were then cultured and passaged in SMM. Saturated cultured were then inoculated in 10% D/G SMM (SMM with 90% of dextrose replaced with galactose) to induce expression of the transgene overnight. Next, 800 μl of cultures normalized OD_{600} to 7 were then pelleted and resuspended in DPBS with or without 100 μM biotin at 30 °C for 6 h rotating in the dark or exposed to light as indicated. After that, samples were kept on ice to stop labeling and washed with DPBS twice. Cells were resuspended with 150 μl of water and 150 μl of 0.6 M NaOH was added. Samples were incubated at room temperature for 5 min and then pelleted. Next, 30 μl of 2× Protein loading buffer was used to resuspend cells and boiled for 5 min at 95 °C. Finally, 15 μl of PBS was then added to dilute the samples.

LOV-Turbo labeling in *E. coli* cytosol

To collect western blot samples of BL21 *E. coli* in Fig. 3b, BL21 containing with the indicated constructs were induced with 1 mM isopropyl-β-D-thiogalactoside overnight in Luria-Bertani media containing selection marker ampicillin. Next, 800 μl of cultures normalized OD_{600} to 3 were pelleted and resuspended in DPBS with 100 μM biotin where indicated. Samples were incubated for 4 h at 37 °C and rotated while covered by aluminum foil in the dark or exposed to light. Bacteria were then pelleted and lysed in 30 μl of 6× protein loading buffer and boiled for 5 min at 95 °C. Samples were then diluted with an additional 50 μl of RIPA buffer.

LOV-Turbo labeling in rat cortical neuron cultures

All procedures were approved and carried out in compliance with the Stanford University Administrative Panel on Laboratory Animal Care, and all experiments were performed in accordance with relevant guidelines and regulations. Before dissection, plates were coated with 0.001% (w/v) poly-L-ornithine (Sigma-Aldrich) in DPBS (Gibco) at room temperature overnight, washed twice with DPBS, and subsequently coated with 5 μg ml^{-1} of mouse laminin (Gibco) in DPBS at 37 °C overnight. Cortical neurons were extracted from embryonic day 18 Sprague Dawley rat embryos (Charles River Laboratories, strain 400) by dissociation in Hank's balanced salt solution (Gibco) supplemented with 1 mM D-glucose and 10 mM HEPES pH 7.2 (Thermo Life Sciences). Cortical tissue was digested in papain according to the manufacturer's protocol (Worthington), then plated onto 0.1 mm thick glass coverslips in neuronal plating medium at 37 °C under 5% CO_2. The neuronal plating medium is 1:1 Advanced DMEM (Gibco): neurobasal (Gibco), supplemented with 2% (v/v) B27 supplement (Life Technologies), 5% (v/v) fetal bovine serum, 1% GlutaMAX (Gibco), 1% penicillin-streptomycin (VWR, 5 units per ml penicillin, 5 μg ml^{-1} streptomycin), 0.1% (v/v) β-mercaptoethanol, 5 ng ml^{-1} recombinant human glial cell line-derived neurotrophic factor (Gibco) and 5 μM TRO19622 (Tocris). Every 3 days after plating, half of the media was removed from each well and replaced with neuronal growth medium. The neuronal growth medium is neurobasal supplemented with 2% (v/v) B27 supplement, 1% GlutaMAX, 50 units per ml penicillin and 50 μg ml^{-1} streptomycin. At 3 days in vitro (DIV), 450 μl of media was removed from each well and replaced with 500 μl of complete neurobasal media supplemented with 10 μM 5-fluorodexoyuridine (Sigma-Aldrich) to inhibit glial cell growth. On DIV 6, each well was infected with 2.5×10^6 vg of concentrated AAV1/2 along with a media change. Neurons were wrapped in aluminum foil and were allowed to express for an additional 5–6 days in the incubator. For Fig. 4a, cells were treated with a final concentration of 50 μM biotin and 500 nM

MitoTracker (Thermo Fisher, M7512), and exposed to 470 nm blue LED light for 2 h in the incubator. Cells were fixed and stained for immunofluorescence detection as described above. For Fig. 3d and Supplementary Fig. 3c, cells were treated with a final concentration of 100 µM biotin and exposed to 470 nm blue LED for 30 min in the incubator. Cells were lysed or fixed for western blot analysis or immunofluorescence detection as described above.

LOV-Turbo labeling in mouse brain

All animal procedures were performed in accordance with Stanford's Institutional Animal Care and Use Committee policies. Here, 8–10 week-old C57BL/6J mice (Jackson Laboratory Strain 000664) were used for all experiments. Mice were group-housed in a 12-hour light and dark cycle (07:00 to 19:00) and given ad libitum food and water. Temperature was maintained between roughly 18 and 23 °C and humidity was kept at 40–60%. While under 2–3% isoflurane anesthesia, mice were stereotaxically injected with 500 nl of AAV1/2 in the primary motor cortex (M1) at the following coordinates relative to bregma: anterior +0.62, lateral −1.5 and ventral −1.0 mm. Mice were allowed to recover for 14 days. Mice were then placed under anesthesia, injected with 0.5 µl of 10 mM biotin at the same stereotaxic coordinates and implanted with a 200 µm diameter optical fiber (Thorlabs) roughly 100 µm above the injection site. A subset of mice also received blue light stimulation through the optical fibers using a patch cable and 470 nm fiber-coupled LED (Thorlabs; 5 mW cm^{-2} of 470 nm light measured at the fiber tip, then 10 Hz pulses, 10 ms pulse width, 10% duty cycle) for 1.5 h. After light treatment, both experimental and control groups of mice were euthanized for tissue collection.

Mice were deeply anesthetized using 1 ml intraperitoneally delivered 2.5% Avertin. They were then quickly perfused with 10 ml of ice-cold PBS, and their brains were immediately dissected and cut in a roughly 1 mm coronal section using a brain block and razor blades on ice. The M1 cortex was micro-dissected from the coronal slice and placed in 200 µl of ice-cold buffer, 50 mM Tris/HCl, pH 7.5, 150 mM NaCl, 1 mM EDTA supplemented with protease inhibitor cocktail and PMSF. Each sample contained M1 dissected from five roughly 1 mm coronal sections. A tissue homogenizer was then used to process the tissue. The samples were lysed by adding 1 ml of ice-cold buffer containing 0.2% SDS, 1% TrixonX-100, and 1% sodium deoxycholate. Samples were incubated with benzonase (50 U ml^{-1}) at 4 °C for 30 min and briefly sonicated for 30 s. Lysates were cleared via centrifugation at 20,000*g* at 4 °C for 30 min, and then processed for western blot analysis as described above.

BRET activation of LOV-Turbo

To generate samples used in Fig. 4g, cells were transiently transfected with V5-NanoLuc-LOV-Turbo-NES fusion as described and induced to express overnight with doxycycline in the dark. Cells were then treated to 100 µM biotin and either kept in the dark, stimulated with 10 min of light or stimulated for 10 min or 1 h by BRET through activation of NanoLuc's bioluminescence with its substrate furimazine (1:100 dilution of Promega nano-Glo Live Assay). After treatment, cells were washed in cold DPBS twice and lysed in RIPA buffer containing protease inhibitor cocktail. Samples were then combined with protein loading buffer and boiled at 95 °C for 5 min for gel loading.

To generate samples used in Fig. 4i, cells were transiently cotransfected with CCR6-NanoLuc-V5 and Myc-Arrestin-LOV-Turbo and induced to express overnight with doxycycline in the dark. Cells were then treated to 100 µM biotin and kept in the dark, stimulated with 10 min of light or stimulated with 1 h of furimazine and with or without CCR6 activation by addition of its substrate CCL20 (0.2 µg ml^{-1}). After treatment, cells were washed in cold DPBS twice and lysed in RIPA buffer containing protease inhibitor cocktail. Samples were then combined with protein loading buffer and incubated at 37 °C for 10 min for gel loading.

LOV-Turbo labeling for pulse-chase proteomics

To generate samples for Fig. 4c and Supplementary Fig. 3f,g, HEK 293T cells expressing LOV-Turbo-NLS plated on human fibronectin-covered glass coverslips were induced to express overnight with doxycycline. Cells were labeled with 100 µM biotin and blue light for 10 min followed by 0, 2, 4 or 8 h chase in the dark in fresh media. Cells were then fixed and processed for immunofluorescence to detect LOV-Turbo-NLS labeling and localization by staining with primary antibody anti-V5 followed by staining with antimouse-AlexaFluor-488, DAPI and neutravidin-AlexaFluor647.

To generate samples for Fig. 4e, HEK 293T cells expressing LOV-Turbo-NES plated 10 cm cell culture dishes were induced to express overnight with doxycycline. Cells were labeled with 100 µM biotin and blue light for 30 min followed by 0- or 2-h chase in the dark in fresh media at either 37 or 42 °C. Cells were collected in 2 ml DPBS. Next, 50 µl was removed and lysed in RIPA buffer containing protease inhibitor cocktail to generate the whole-cell lysate samples. The remainder was processed for nuclear fractionation. The nuclear fraction was then lysed in 500 µl of RIPA buffer containing protease inhibitor cocktail and benzonase. Then, 50 µl were removed to generate the nuclear lysate samples. The remainder was processed for streptavidin enrichment. All samples from the whole-cell lysate, nuclear lysate, and streptavidin enrichment were analyzed by western blotting using streptavidin, anti-importin-α antibody and anti-HSP70 antibody.

Streptavidin enrichment of LOV-Turbo labeled material

Streptavidin enrichment was performed following the protocol in Cho et al.[7] Streptavidin beads were washed with 1 ml of RIPA buffer twice before adding to the cell lysate and incubated overnight at 4 °C overnight or 1 h at room temperature, rotating. Beads were then washed thrice with 1 ml of RIPA buffer, followed by washes of 1 M KCl, 0.1 M Na_2CO_2 and 2 M urea in 10 mM Tris-HCl (pH 8). Beads were then washed with 1 ml of RIPA three more times. Then, proteins were eluted from beads using 3× protein loading buffer containing 2 mM biotin and 20 mM dithiothreitol (DTT) at 95 °C for 5 min.

Nuclear fractionation

Nuclear fractionations were performed following the protocols and suggestions published by Gagnon et al.[54], and Senichkin et al.[55] Cells were collected in DPBS with some aliquoted for whole-cell lysate samples then pelleted at 500*g* at 4 °C for 2 min. Then, 1 ml of hypotonic lysis buffer (20 mM Tris (pH 7.5), 5 mM KCl, 3 mM $MgCl_2$, 10% glycerol, 0.5% NP-40 and protease inhibitor cocktail) was used to resuspend 75 mg of cells and incubated on ice for 10 min. Cells were briefly vortexed and centrifuged at 500*g* for 5 min at 4 °C. Then, 870 µl of the supernatant was transferred to a new tube and combined with 25 µl of 5 M NaCl to generate the cytoplasmic fraction. The remaining supernatant was discarded and the pellet was resuspended in 1 ml of hypotonic lysis buffer. The nuclear fraction was pelleted at 500*g* for 2 min and then washed in cold isotonic wash buffer (20 mM Tris-HCl (pH 7.5), 100 mM KCl, 3 mM $MgCl_2$, 10% glycerol, 0.5 mM DTT, 0.5% NP-40 and protease inhibitor cocktail). This washing step with the isotonic wash buffer was performed once more. Then, the nuclear pellet was lysed in RIPA buffer containing benzonase at 1,000 U ml^{-1} (Millipore).

Mitochondrial fractionation

Mitochondria fractionations were performed using the Pierce Mitochondria Isolation Kit for Tissue with the following modifications. Cells were collected in DPBS. Before fractionation, a subset of cells was aliquoted to generate the whole-cell lysate samples. Cells were pelleted at 700*g* for 2 min at 4 °C. The supernatant was removed, and the cell pellet was resuspended in 800 µl of Reagent A supplemented with a protease inhibitor cocktail for 2 min. The cells were then lysed using a Dounce tissue grinder (Kimble) 15 times and then transferred into a 2 ml tube. Then 800 µl of Reagent C supplemented with protease inhibitor

cocktail was added. The grinder was washed with 200 µl of Reagent A, that was then added back to the cells. The cells were then centrifuged at 700*g* for 10 min at 4 °C and the supernatant was transferred to a new tube. This step was repeated until a pellet was no longer visible following centrifugation. Proteinase K was added at 10 U ml^{-1} for 20 min at 4 °C to remove proteins on the outside the mitochondria, then PMSF was supplemented at 1 mM to inhibit it. The mitochondrial fraction was pelleted at 3,000*g* for 15 min and the pellet was washed twice with Reagent C, centrifuging after each wash at 12,000*g* for 5 min. Finally, the mitochondrial pellet was lysed in RIPA lysis buffer.

Sample preparation for mass spectrometry

To generate samples for ERM to mitochondria translocation profiling, cells stably expressing LOV-Turbo-ERM or LOV-Turbo-NES were plated on 127.5 × 85.5 mm plates and induced with doxycycline overnight. Cells were treated with 100 µM biotin and stimulated with light or kept in the dark for 1 h. Biotin media was washed out with DPBS three times and then replaced with fresh media containing 1 µM FCCP, 100 nM thapsigargin or no drug for 8 h. Cells were then collected and fractionated for their mitochondria and lysed in 500 µl of RIPA buffer containing protease inhibitor cocktail. Mitochondrial lysates were flash-frozen with liquid nitrogen and kept at −80 °C until ready to proceed to streptavidin enrichment. For each channel, samples collected from two plates were combined. Combined 1 ml of mitochondrial lysate were then incubated with 50 µl of streptavidin beads for enrichment and incubated with the beads overnight at 4 °C. After washing, 2.5% of each sample was removed to be eluted with protein loading buffer and checked by silver stain (Pierce) for the presence of sufficient proteins. The remaining beads were washed twice with 75 mM NaCl in 50 mM Tris-HCl (pH 8) and then flash-frozen in 50 µl of the buffer.

To generate samples for ERM to nucleus translocation profiling, cells stably expressing LOV-Turbo-ERM or LOV-Turbo-NES were plated on 127.5 × 85.5 mm plates and induced with doxycycline overnight. Cells were treated with 100 µM biotin and stimulated with light or kept in the dark for 30 min. Biotin media was replaced with fresh media containing 2 µg ml^{-1} tunicamycin for 2 h. Cells were then collected and fractionated for their nucleus and lysed in 500 µl of RIPA buffer containing protease inhibitor cocktail. For each channel samples collected from two plates were combined. Clarified lysates were incubated with 35 µl of streptavidin beads for enrichment and incubated for 1 h at room temperature. After washing, 2.5% of each sample was removed to be eluted with protein loading buffer and checked by silver stain (Pierce) for the presence of sufficient proteins. The remaining beads were washed twice with 75 mM NaCl in 50 mM Tris-HCl (pH 8) and then flash-frozen in 50 µl of the buffer.

On-bead trypsin digestion of biotinylated proteins

Samples collected and enriched with streptavidin magnetic beads were washed twice with 200 µl of 50 mM Tris-HCl buffer (pH 7.5), transferred into new 1.5-ml Eppendorf tubes, and washed twice more with 200 µl of 50 mM Tris (pH 7.5) buffer. Samples were incubated in 0.4 µg trypsin in 80 µl of 2 M urea per 50 mM Tris buffer with 1 mM DTT, for 1 h at room temperature while shaking at 1,000 rpm. Following predigestion, 80 µl of each supernatant was transferred into new tubes. Beads were then incubated in 80 µl of the same digestion buffer for 30 min while shaking at 1,000 rpm. Supernatant was transferred to the tube containing the previous elution. Beads were washed twice with 60 µl of 2 M urea per 50 mM Tris buffer and these washes were combined with the supernatant. The eluates were spun down at 5,000*g* for 30 s and the supernatant was transferred to a new tube. Samples were reduced with 4 mM DTT for 30 min at room temperature, with shaking. Following reduction, samples were alkylated with 10 mM iodoacetamide for 45 min in the dark at room temperature. An additional 0.5 µg of trypsin was added and samples were digested overnight at room temperature while shaking at 700*g*. Following overnight digestion, samples were acidified (pH less than 3) with neat formic acid, to a final concentration of 1% formic acid. Samples were spun down and desalted on C18 StageTips as previously described. Eluted peptides were dried to completion and stored at −80 °C.

TMT labeling and fractionation

Desalted peptides were labeled with TMTpro (18-plex) reagents (Thermo Fisher Scientific). Peptides were resuspended in 80 µl of 50 mM HEPES and labeled with 20 µl of 25 mg ml^{-1} TMTpro18 reagents in ACN. Samples were incubated at room temperature for 1 h with shaking at 1,000 rpm. TMT reaction was quenched with 4 µl of 5% hydroxylamine at room temperature for 15 min with shaking. TMT-labeled samples were combined, dried to completion, reconstituted in 100 µl of 0.1% formic acid and desalted on StageTips.

TMT-labeled peptide sample was fractionated by basic reverse phase (bRP) fractionation. StageTips packed with two disks of SDB-RPS (Empore) material. StageTips were conditioned with 100 µl of 100% MeOH, followed by 100 µl of 50% MeCN/0.1% formic acid and two washes with 100 µl of 0.1% formic acid. Peptide samples were resuspended in 200 µl of 1% formic acid (pH < 3) and loaded onto StageTips. Eight step-wise elutions were carried out in 100 µl of 20 mM ammonium formate buffer with increasing concentrations of 5, 7.5, 10, 12.5, 15, 20, 25 and 45% MeCN. Eluted fractions were dried to completion.

LC–MS/MS

All peptide samples were separated with an online nanoflow Proxeon EASY-nLC 1200 ultrahigh-performance liquid chromatography system (Thermo Fisher Scientific) and analyzed on an Orbitrap Exploris 480 mass spectrometer (Thermo Fisher Scientific). In this set up, the LC system, column and platinum wire used to deliver electrospray source voltage were connected via a stainless-steel cross (360 mm, IDEX Health & Science, UH-906x). The column was heated to 50 °C using a column heater sleeve (Phoenix-ST). Each sample was injected onto an in-house packed 27 cm × 75 µm internal diameter C18 silica picofrit capillary column (1.9 mm ReproSil-Pur C18-AQ beads, Dr. Maisch GmbH, r119.aq; PicoFrit 10 µm tip opening, New Objective, PF360-75-10-N-5). Mobile phase flow rate was 200 nl min^{-1}, composed of 3% acetonitrile/0.1% formic acid (Solvent A) and 90% acetonitrile/0.1% formic acid (Solvent B). The 154-min LC–MS/MS method used the following gradient profile: (min:%B) 0:2;2:6; 122:35; 130:60; 133:90; 143:90; 144:50; 154:50 (the last two steps at 500 nl min^{-1} flow rate). Data acquisition was done in the data-dependent mode acquiring HCD MS/MS scans (r = 45,000) after each MS1 scan (r = 60,000) on the top 12 most abundant ions using a normalized MS1 AGC target of 100% and an MS2 AGC target of 50%. The maximum ion time used for MS/MS scans was 120 ms; the HCD-normalized collision energy was set to 32; the dynamic exclusion time was set to 20 s, and the peptide match and isotope exclusion functions were enabled. Charge exclusion was enabled for charge states that were unassigned, 1 and more than 6.

Analysis of mass spectrometry data (peptide level, protein level)

Mass spectrometry data was processed using Spectrum Mill v.7.11 (proteomics.broadinstitute.org). For all samples, extraction of raw files retained spectra within a precursor mass range of 600–6,000 Da and a minimum MS1 signal-to-noise ratio of 25. MS1 spectra within a retention time range of ±45 s, or within a precursor m/z tolerance of ±1.4 m/z were merged. MS/MS searching was performed against a human Uniprot database with a release date of 28 December 2017. Digestion parameters were set to 'trypsin allow P' with an allowance of four missed cleavages. The MS/MS search included fixed modification of carbamidomethylation on cysteine. TMTpro18 was searched using the full-mix function. Variable modifications were acetylation and oxidation of methionine. Restrictions for matching included a minimum matched peak intensity of 30% and a precursor and product mass tolerance of ±20 ppm.

Peptide spectrum matches were validated using a maximum false discovery rate threshold of 1.2% for precursor charges 2 to 6 within each LC–MS/MS run. Protein polishing autovalidation was further applied to filter the peptide spectrum matches using a target protein score threshold of 9. TMTpro18 reporter ion intensities were corrected for isotopic impurities in the Spectrum Mill protein/peptide summary module using the afRICA correction method that implements determinant calculations according to Cramer's Rule. We required fully quantified unique human peptides for protein quantification. We used the Proteomics Toolset for Integrative Data Analysis (Protigy, v.1.0.4, Broad Institute, https://github.com/broadinstitute/protigy) to calculate moderated *t*-test *P* values for regulated proteins.

Cloning

For cloning, fragments were PCR amplified using Q5 polymerase (NEB) and vectors were digested using restriction enzymes. All fragments were gel purified and ligated using Gibson assembly (NEB), then transformed into stable competent *E. coli* (NEB). LOV-Turbo gene was codon optimized for human via GenSmart. Below is the complete amino acid sequence of our final optimized LOV-Turbo:

KDNTVPLKLIALLANGEFHSGEQLGETLGMSRAAINKHIQTLRDWGVDVFSVPGKGYSLPEPIPLLNAKQIQGQLEFRATTLERIEKSFVITDPRLPDNPIIFVSDSFLQLTEYSREEILGRNCRFLQGPETDRATVRKIRDAIDNQTEVTVQLINYTKSGKKFWNVFHLQPMRDYKGDVQYFIGVQLDGTERLHGAAEREAVCLVKKTAFQIAVAVLPVVDSTNQYLLDRIGELKSGDACIAEYQQAGRGSRGRKWFSPFGANLYLSMFWRLKRGPAATGLGPVIGIVMAEALRKLGVDKVRVKWPNDLYLQDRKLAGILVELAGITGDAAQIVIGAGINVAMRRVEESVVNQGWITLQEAGVNLDRNTLAATLIRELRAALELFEQEGLAPYLPRWEKLDNFINRPVKLIIGDKEILGISRGIDKQGALLLEQDGVIKPWMGGEISLRSAEK

TurboID(1–76 amino acids (aa), T52S, L73Q)-hLOV1-TurboID(81–321aa, I147T, A166V, I231V, F286L)

To target LOV-Turbo to various subcellular compartments, we created genetic fusions to a nuclear export signal (NES, C-terminal), nuclear localization signal (NLS, C-terminal), SEC61B protein (to target to ERM facing cytosol, C-terminal), COX4I1 mitochondrial targeting sequence (MTS) (to target to the mitochondrial matrix (1) in Fig. 2d, N-terminal), COX4I1 MTS-NES (to target to the mitochondrial matrix (2) in Fig. 2d, N-terminal for COX4I1 MTS and C-terminal for NES), 3× COX8A MTS-NES (to target to the mitochondrial matrix (3) in Fig. 2d, N-terminal for 3× COX8A MTS and C-terminal for NES) or AKAP1 transmembrane domain (to target to the outer mitochondrial membrane, N-terminal). For mitochondrial matrix targeting, COX4I1 worked the best. Specific amino acid sequences of targeting peptides are given in the Supplementary Information.

Reporting summary

Further information on research design is available in the Nature Portfolio Reporting Summary linked to this article.

Data availability

The data associated with this study are available in the article and the Supplementary Information. The original mass spectra, spectral library and the protein sequence database used for searches have been deposited in the public proteomics repository MassIVE (http://massive.ucsd.edu) and are accessible at ftp://massive.ucsd.edu/MSV000090683/. Additional data beyond that provided in the figures and Supplementary Information are available from the corresponding author on request.

References

52. Chao, G. et al. Isolating and engineering human antibodies using yeast surface display. *Nat. Protoc.* **1**, 755–768 (2006).
53. Colby, D. W. et al. Engineering antibody affinity by yeast surface display. *Methods Enzymol.* **388**, 348–358 (2004).
54. Gagnon, K. T., Li, L., Janowski, B. A. & Corey, D. R. Analysis of nuclear RNA interference in human cells by subcellular fractionation and Argonaute loading. *Nat. Protoc.* **9**, 2045–2060 (2014).
55. Senichkin, V. V., Prokhorova, E. A., Zhivotovsky, B. & Kopeina, G. S. Simple and efficient protocol for subcellular fractionation of normal and apoptotic cells. *Cells* **10**, 852 (2021).

Acknowledgements

Rat cortical neurons were a kind gift from M. Lin (Stanford University). We thank J. Reinstein (Max Planck Institute) for helpful feedback. This work was supported by the NIH (grant nos. R01-DK121409 and RC2DK129964 to A.Y.T., R01-OD026223 to A.Y.T. and S.A.C. and T32GM007276 to J.S.C.), the Stanford Wu Tsai Neurosciences Institute (A.Y.T.), the National Science Foundation (NeuroNex grant no. 2014862 to A.Y.T. and GRFP DGE-1656518 to J.S.C.), the National Research Foundation of Korea grant no. NRF-2019R1A6A3A03033677 (S.-Y.L.), the Stanford Gerald J. Lieberman Fellowship (J.S.C.) and the Burroughs Wellcome Fund grant no. CASI 1019469 (C.K.K.). A.Y.T. is a Chan Zuckerberg Biohub – San Francisco Investigator.

Author contributions

S.-Y.L. and A.Y.T. conceived this project. S.-Y.L., J.S.C. and A.Y.T. designed experiments and analyzed all the data except those noted. S.-Y.L. and J.S.C. performed all experiments, unless otherwise noted. N.D.U., C.X. and S.A.C. performed post-streptavidin-enrichment sample processing, mass spectrometry, and initial data analysis. B.Z. and S.-Y.L. performed the mouse brain experiments. C.K.K., K.F.C. and S.-Y.L. performed cultured rat cortical neuron experiments. H.R. and S.-Y.L. performed BRET experiments. S.-Y.L., J.S.C. and A.Y.T. wrote the paper with input from all authors.

Competing interests

S.-Y.L., J.S.C. and A.Y.T. have filed a patent application covering some aspects of this work (US Provisional Patent Application No. 63/488,940; CZ SF ref. CZB-273S-P1; Stanford ref. S22-487; KT ref. 110221-1361830-009500PR). The remaining authors declare no competing interests.

Additional information

Supplementary information The online version contains supplementary material available at https://doi.org/10.1038/s41592-023-01880-5.

Correspondence and requests for materials should be addressed to Alice Y. Ting.

Peer review information *Nature Methods* thanks Angelos Constantinou, Tatsuya Sawasaki and the other, anonymous, reviewer(s) for their contribution to the peer review of this work. Primary Handling Editor: Rita Strack, in collaboration with the *Nature Methods* team.

Reprints and permissions information is available at www.nature.com/reprints.